Magnetic Fabric Signature within a Thrust Imbricate; an analogue modelling approach

Thorben Schöfisch[1], Hemin A. Koyi[1], and Bjarne Almqvist[2]

[1]Uppsala University
[2]Uppsala Universitet

November 21, 2022

Abstract

In this study, we report results from three analogue models with similar initial setup and different amounts of bulk shortening, to simulate a development of a pop-up structure in fold-and-thrust belts at different stages. Samples are taken in different places of the deformed models for analysis using anisotropy of magnetic susceptibility. Shortening of the models resulted in the formation of a pop-up structure, which is bounded by backthrust(s) and complex forekink zone(s). Several forethrusts at different degrees of maturity developed in front of the pop-up structure. Three distinct types of magnetic fabric can be identified throughout the models: (i) a compactional oblate fabric that changes as function of distance towards a localized deformation zone (e.g., thrust or kinkzone), (ii) a thrust-induced fabric with magnetic foliation parallel to the thrust surface, and (iii) a complex forekink zone fabric with broad girdle distributions of principal axes and magnetic lineation perpendicular to shortening direction. The latter indicate interplay between folding and thrusting of the shortened sand layers. Additionally, a decrease in degree of anisotropy with appearance of a quantitatively more prolate fabric can be observed towards the thrusts and kinkzones. Additionally at thrusts, a variation in strain is reflected by the magnetic fabric and can be inherited in a thrust-induced fabric. In conclusion, strain is changing as function of distance towards localized deformation zones with characteristic fabric, and differences in magnetic fabric are distinct between data away and within deformation zones as deformation zones mature.

Magnetic Fabric Signature within a Thrust Imbricate; an analogue modelling approach

T. Schöfisch[1], H. Koyi[1*] , and B. Almqvist[1]

[1]Hans Ramberg Tectonic Laboratory, Department of Earth Sciences, Uppsala University, Villavägen 16, 752 36 Uppsala, Sweden.

Corresponding author: Thorben Schöfisch (thorben.schofisch@geo.uu.se)

*current address: Department of Earth Sciences, Khalifa University of Science and Technology, Abu Dhabi, United Arab Emirates

Key Points:

- Anisotropy of magnetic susceptibility as strain indicator within three analogue models simulating a development of a pop-up structure
- Characteristic sets of magnetic fabric are developed for each structure in the models, which reveal deformation in more detail
- Gradients in changes in magnetic fabric are recognized as function of distance towards a thrust or kinkzone

Abstract

In this study, we report results from three analogue models with similar initial setup and different amounts of bulk shortening, to simulate a development of a pop-up structure in fold-and-thrust belts at different stages. Samples are taken in different places of the deformed models for analysis using anisotropy of magnetic susceptibility. Shortening of the models resulted in the formation of a pop-up structure, which is bounded by backthrust(s) and complex forekink zone(s). Several forethrusts at different degrees of maturity developed in front of the pop-up structure. Three distinct types of magnetic fabric can be identified throughout the models: (i) a compactional oblate fabric that changes as function of distance towards a localized deformation zone (e.g., thrust or kinkzone), (ii) a thrust-induced fabric with magnetic foliation parallel to the thrust surface, and (iii) a complex forekink zone fabric with broad girdle distributions of principal axes and magnetic lineation perpendicular to shortening direction. The latter indicate interplay between folding and thrusting of the shortened sand layers. Additionally, a decrease in degree of anisotropy with appearance of a quantitatively more prolate fabric can be observed towards the thrusts and kinkzones. Additionally at thrusts, a variation in strain is reflected by the magnetic fabric and can be inherited in a thrust-induced fabric. In conclusion, strain is changing as function of distance towards localized deformation zones with characteristic fabric, and differences in magnetic fabric are distinct between data away and within deformation zones as deformation zones mature.

Plain Language Summary

Deformation within fold-and-thrust belts occurs as thrusting (displacement along weak zones), folding (bending of rock units) and internal deformation. The internal deformation, like compaction and grain realignment, is hard to analyze by the naked eye. Fortunately, the magnetic properties of grains can be measured and provide information of grain realignment within an imbricate. In this study, we combine analogue modelling with magnetic analysis to track the internal deformation of imbricates in detail. We modelled imbricates and analyzed the magnetic fabric within the models. Our observations show a gradual change in magnetic fabric within an imbricate towards thrusts and kinkzones, which bound the imbricate, showing increasing deformation. At the thrusts, the magnetic fabric aligns parallel to the thrust surface, whereas in the kinkzone a complex interplay between folding and thrusting is revealed. Our results can be compared to natural examples, as observation from models and published natural analogies are comparable. Our study provides insights into the strain distribution and gradients within imbricates.

1 Introduction

Three main components take up deformation in fold-and-thrust belts (FTBs); layer-parallel shortening (LPS), folding and faulting. In FTBs, most structures like thrusts and folds can be mapped and analyzed with different techniques by their optical appearance (e.g., Ramsay and Huber, 1983). However, in the absence of strain markers, penetrative strain (i.e., layer-parallel shortening), which is not always easy to quantify in the field, can also be quantified by focusing on an intrinsic property of the rocks, i.e., their magnetic susceptibility. The anisotropy of magnetic susceptibility (AMS) has proven to be a useful tool to study strain in different tectonic regimes and lithologies (e.g., Graham, 1966; Hrouda, 1982; Averbuch et al., 1992; Borradaile and Henry, 1997; Bakhtari et al., 1998; Saint-Bezar et al.,2002; Borradaile and Jackson, 2010; Ferré et al., 2014; Parés, 2015).

Quantifying penetrative strain in fold-thrust belts is not always possible due to lack of strain markers and outcrops and difficulty of accessing deeper levels. However, in analogue models, where initial and subsequent deformation stages are well documented and different parts are accessible, strain partitioning in model FTBs and accretionary wedges can be quantified, which assists in interpreting field observations and the development of FTBs (e.g., Davis et al., 1983; Dahlen et al., 1984; Mulugeta, 1988; Mulugeta and Koyi, 1992; Liu et al., 1992; Koyi, 1995; Gutscher et al., 1996; Storti et al., 2000; Koyi et al., 2003; Sans et al., 2003; Adam et al., 2005; Graveleau et al., 2012; Dotare et al., 2016). It has been reported that in most of the model studies simulating FTBs, the granular material (simulating sedimentary rocks) is compacted, and the deformation front propagates from the backstop towards the foreland of the model. Shear bands precede thrust initiation (Dotare et al., 2016) and with further shortening thrusts act as ramps (e.g., Suppe, 1983) where strain is refracted into the hangingwall (Maillot and Leroy, 2003; Maillot and Koyi, 2006; Koyi and

Maillot, 2007). Imbricates between the thrusts deform internally (Koyi, 1995) and overall strain varies both with time and depth (Mulugeta and Koyi, 1992; Koyi et al., 2003). To monitor and quantify penetrative deformation in analogue models, passive markers printed on the surface of the models are monitored by photogrammetry or laser scanning (reviews by Koyi, 1997; Graveleau et al., 2012; Schellart and Strak, 2016). LPS in models is estimated by cross-section balancing and area calculation (e.g., Koyi et al., 2003; Groshong, 2019), analysis of surface deformed strain markers and volumetric strain (Nilforoushan et al., 2008). Recently, AMS has also been introduced in analogue modelling to quantify strain in models simulating FTBs (Almqvist and Koyi, 2018). In FTBs, the evolution of the magnetic fabric depends on the amount of shortening and location within a FTB. With increasing strain, a primary fabric, i.e., sedimentary fabric, will be overprinted to a completely reoriented tectonic fabric. A mixture of magnetic fabric patterns between primary and tectonic fabric indicates an intermediate fabric, that results from a moderate tectonic overprint of the sedimentary fabric. Intermediate and tectonic magnetic fabric are typical in FTBs and paths in strain change described by tectonic overprint derive from field observations (e.g., Graham, 1966; Borradaile and Tarling, 1981; Kligfield et al., 1981; Averbuch et al., 1992; Bakhtari et al., 1998; Parés et al., 1999; Hirt et al., 2004). A similar magnetic fabric evolution with increasing strain, as seen from field data, is observed in analogue models (Almqvist and Koyi, 2018), with the possibility to differentiate between fabric influenced by thrusting and by grain reorientation due to compaction (Schöfisch et al., 2021).

As a continuation of such modelling studies, in this study, we use the results of a series of shortened sandbox models simulating the evolution of a pop-up structure at different amount of bulk shortening, to investigate the evolution of the magnetic fabric, mainly within an imbricate and at the developed structures. Specifically, the aim of this study is to describe the strain distribution within a pop-up structure and compare the magnetic fabric that develops at different stages of finite strain across the imbricate.

2 Methods

2.1 Model setup and sampling

Three models (A, B, and C) with a similar setup are shortened to different extent in order to analyze the magnetic fabric along thrust faults at different stages that are associated with a development of a pop-up structure (Table 1). To initiate a pop-up structure bounded by active back- and forethrusts, an artificial wedge is sieved and built on top of the model next to the backstop in models A and C. In Model B, a basal plate is attached to the backstop, as a velocity discontinuity, to transmit shortening away from the backstop and initiate a boxfold in the middle of the model away from the backstop. To increase sampling capacity and target individual parts of the boxfold, the models were thick (8 cm) and had an initial dimension of 71x30 cm (Fig. 1). Loose sand was mixed with magnetite grains (<0.1vol%) of the same grain size (0.124-0.356 mm) to enhance magnetic susceptibility. This mixed composition (cohesion $\mu = 0.49$) was used to construct layers that were scraped to an individual thickness of one centimeter each. Between each 1 cm-thick layer, a thin marker horizon is sieved using different colored sand. To monitor surface deformation, a colored grid of circles is imprinted on the model surface by sieving. After shortening, the models are carefully wetted, and vertical sections are taken parallel to the shortening direction (Table 1). Each section is photographed, and oriented cubic samples (volume 2.2 cm^3) are taken across the sections in specific parts of the structure (forethrust, backthrust, forekink zone, crestal areas, undeformed part in the foreland, etc.) for AMS analyses.

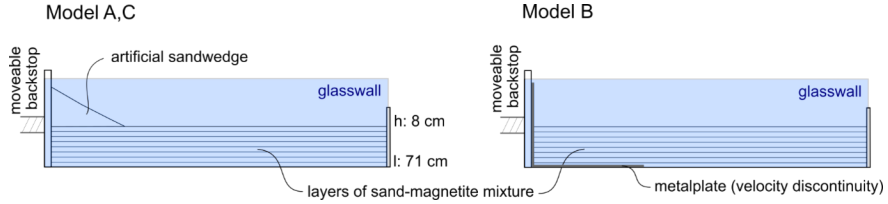

Figure 1: Sketch of model setups. A pre-existing wedge was placed next to the backstop on top of the surface of models A and C. In Model B, a metal plate that moved with the backstop was used as velocity

discontinuity.

Table 1: Overview of setup of the three models. The three models share the same thickness and lateral dimensions but vary in the amount of bulk shortening and sampling.

	bulk shortening	setup variation	sections/samples
Model A	12 cm = 16%	artificial wedge on top of model next to backstop; 7x12 cm, slope: 30°	8 / 289
Model B	17.5 cm = 24.5%	velocity discontinuity by underlying moving metal plate; length: 20 cm	7 / 320
Model C	24 cm = 34%	artificial wedge on top of model next to backstop; 4x8 cm; slope: 26°	5 / 170

2.2 AMS measurements and fabric evolution

AMS measurements were performed with a MFK1-FA Kappabridge (Agico Inc.) using an AC field strength of 200 A/m and a frequency of 976 Hz. From each measurement, the bulk orientation of the principal axes of susceptibility (k_{max} [?] k_{int} [?] k_{min}) of magnetite grains within one sample is calculated and plotted on a lower-hemisphere equal-area projection with the backstop defining the North. Note that the matrix sand, consisting mainly of weakly diamagnetic quartz, is considered to have a negligible contribution to the AMS compared to the magnetite. Furthermore, the principal axes define an ellipsoid, which can be described by the shape of anisotropy ($T = [2n_{int}\ n_{max}\ n_{min}]/[n_{max}\ n_{min}]$) and degree of anisotropy ($Pj = exp\{2(n_{max}\ n_{mean}) + (n_{int}\ n_{mean}) + (n_{min}\ n_{mean})]\}$) with $n_{max} = ln(k_{max})$,$n_{int} = ln(k_{int})$, $n_{min} = ln(k_{min})$, and $n_{mean} = (n_{max} + n_{int} + n_{min})/3$(Jelinek, 1981; Hrouda, 1982). The shape of anisotropy (T) ranges from T = -1 for prolate, T = 0 for neutral to T = +1 for oblate ellipsoids. The degree of anisotropy describes a ratio between the principal axes, hence a change in the alignment of the magnetic grains (magnetite in this model) within a sample will result in a different degree of anisotropy (Hrouda, 1982), e.g., high values indicate a preferred orientation. Analyzing the magnetic fabric throughout the model enables a description of strain changes due to principal axes rotation and it is used to describe a strain path from an oblate depositional fabric towards an intermediate and tectonic fabric with lower Pj and occurrence of more prolate susceptibility ellipsoids (e.g., Kligfield et al.,1981; Rochette et al., 1992; Borradaile and Henry, 1997; Bakhtari et al., 1998). Note that since we neither model ductile deformation, grain fracturing nor recrystallisation, which influence the bulk orientation of the magnetic fabric in cleavages zones (Borradaile and Tarling, 1981; Hirt et al., 2004; Ferré et al., 2014), the magnetic fabric development is limited to rigid body rotation of grains in our models. However, a reworking of the magnetic fabric due to rigid body rotation caused by an increase in LPS, folding and thrusting are often interpreted for FTBs (e.g., Averbuch et al., 1992; Borradaile and Henry, 1997; Bakhtari et al., 1998; Saint-Bezar et al., 2002; Burmeister et al., 2009) and are observed in analogue models (Almqvist and Koyi, 2018; Schöfisch et al., 2021).

3 Results

3.1 Model kinematics and evolution

The three models (Models A, B and C) are shortened to different amounts (12 cm, 17.5 cm, and 24 cm, respectively) (Table 1), but share a relatively similar evolution and comparable development of structures. The main structure that developed during the shortening of the models is a pop-up structure with a well-defined backthrust and a broad forekink zone (Figs. 2a, b, and c). In addition to the pop-up structure, the models developed other structures in their foreland. For example, in front of the pop-up structure in Model A (16% bulk shortening), two new forekinks were initiated as indicated by bending of the surface markers and slight increase in topography (dashed lines in Fig. 2b). These forekinks represent an early stage of forethrust creation. In Model B (24.5% bulk shortening), an additional forethrust (FT1) developed simultaneously with the splay of the backthrust (BT) of the major pop-up structure. Farther into the foreland of Model B, a second forethrust (FT2) formed, represented by a mm-scale fore-kink (Fig. 2b). However, compared to models A and B, Model C (34% bulk shortening) developed a more complex set of structures (Fig. 2c). In this model, a "lower" backthrust (BT1) formed simultaneously with the "upper" forekink zone (FKZ1). At a later stage, an "upper" gently-dipping backthrust (BT2) formed and uplifted FKZ1. Simultaneously

with initiation of BT2, a "lower" forekink zone formed (FKZ2). With further shortening, a second pop-up structure formed in the foreland. This additional foreland-pop-up consists of a narrower forekink zone (FKZ3) and a foreland-backthrust (BT3). This BT3 offsets the upper layers of the FKZ2, which in turn is offset by a forethrust (FT) that initiated during further shortening (after 21 cm of shortening, representing 90% of final bulk shortening of Model C). This FT, located beneath FKZ2, splayed and is related to the deformation of the main pop-up structure, where a new backthrust is about to form above BT2 as counterpart (Fig. 2c, dashed red line in Model C above BT 2) (Fig. 2c). Overall, the three models show a similar evolution of a pop-up structure at different stages of shortening (Figs. 2a, b, and c). Faults and kinks in each model steepen with depth and displacement along all faults decreases with depth (Figs. 2d, e, and f).

3.2 Cross-section balancing

During shortening of the models, strain is partitioned between the three deformation components: layer-parallel shortening (LPS), folding, and thrusting. The amount of deformation taken up by thrusting and folding is proportional to the percentage of bulk shortening. However, most of the strain in all models is accommodated by LPS, i.e., penetrative strain (Figs. 2d, e, and f). Even though LPS increases with bulk shortening, its contribution to the overall strain decreases relative to that of folding and thrusting with progressive bulk shortening. In general, the amount of LPS and folding are changing with depth in all models, whereas thrusting decreases (Figs. 2d, e, and f). Additionally, the distribution of strain and its trend with depth is different in Model B compared to models A and C (Figs. 2d, e, and f). In Model B, LPS decreases from the surface to layer 4 and then increases again towards the deeper layers (Fig. 2e), whereas the opposite is the case for folding. Thrusting in Model B mainly decreases with depth as seen in models A and C (Figs. 2d, e, and f).

3.3 Magnetic fabric

In the three models, 779 samples were taken and analyzed for AMS signature (Table 1). We separated the datasets from the models by their location relative to the main structures (thrusts and forekink zone) and describe the characteristic magnetic fabric in detail in the following sections. The distance of a sample to a thrust or a kinkzone is measured by using the center of the sample. Consequently, we assume that samples, whose centers are lying in a range of 0.8 cm (length from center to corner of the cubic samples) to a thrust or kinkzone, are carrying a signal that is attributed to thrust or kinkzone and are summarized within the datasets showing magnetic fabrics of such a structure. The complete dataset is provided in the data repository (Schöfisch, 2021) and an overview of AMS distribution across the pop-up structures are presented as supplementary material (S1-S8).

3.3.1 M*agnetic fabric away from thrust and kinkzone*

An oblate shape of anisotropy, where kmin axes are clustered vertically relative to bedding, is observed in all models in areas away from a thrust or kinkzone, i.e., the footwall of the backthrusts next to the backstop, the interlimb zone between the main backthrust and main forekink zone, and the areas between the "minor foreland" thrusts in front of the main forekink zones (Fig. 3). Both kmax and kint define a horizontal to subhorizontal magnetic foliation around the primitive circle parallel to the sand layers in these areas, where kmax is generally aligned along the model north (towards backstop)-south axis, and kint clusters mainly in the east and

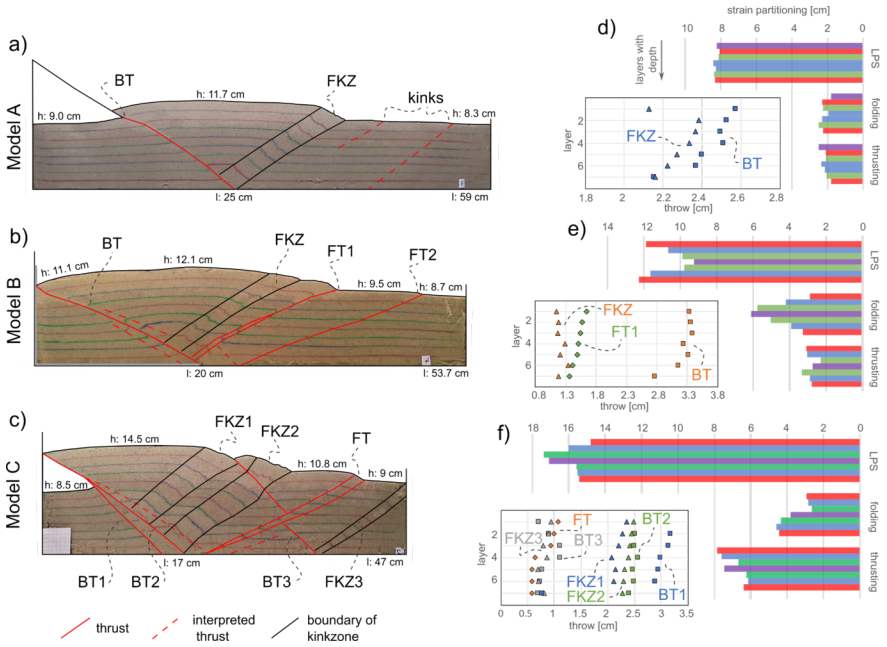

Figure 2: Three models A,B,C are shortened to different amount of bulk shortening (16%, 24.5%, 34%). They show the evolution of a pop-up structure. a,b,c) show representative cross-sections for each model. d,e,f) show the restoration of cross-sections, which provide a partitioning of strain. Additionally, the heave at major structures is plotted for each layer counting from the top.

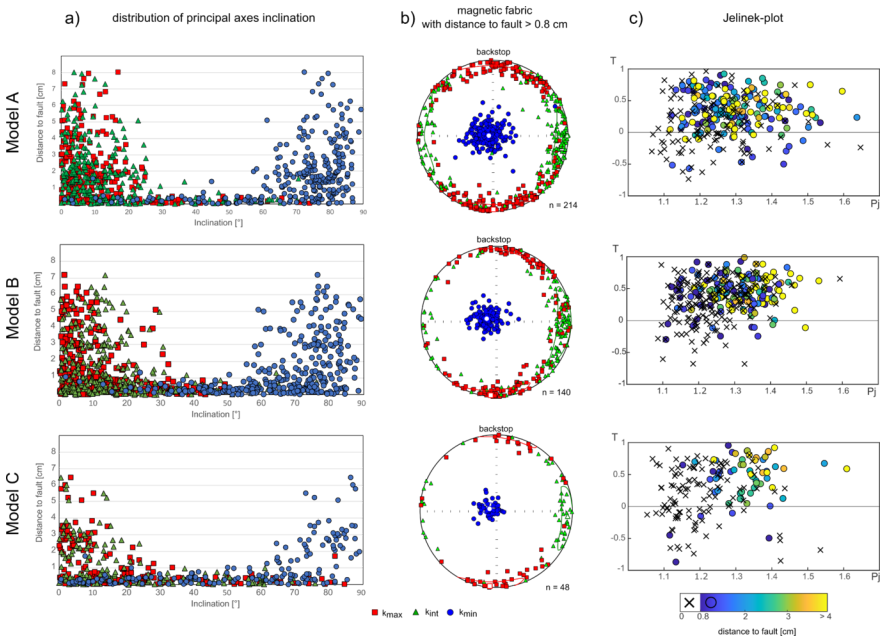

Figure 3: a) plots of the inclination of the principal axes (kmax [?] kint [?] kmin) as a function of distance to a thrust or kinkzone. b) equal-area projection showing distribution of principal axis for samples with a distance > 0.8 cm to a thrust or kinkzone with backstop to the North. c) illustrates the distribution of degree

and shape of anisotropy using the Jelinek-plot. Circles coincide with samples taken away from a thrust of kinkzone, whereas crosses represent data from thrust and kinkzone.

west direction (Fig. 3b). The degree of anisotropy in these areas lies in the interval between 1.1 [?] Pj [?] 1.6 (Fig. 3c).

All three models show a general trend in principal axes rotation as a function of distance to a thrust or kinkzone (Fig. 3a). The closer the sample is to such a structure, the larger is the variety of inclinations of the principal axes, e.g., kmax and kint axes rotate from mainly horizontal inclinations to broad range of inclinations (Fig. 3a). The opposite is observed for the inclination of kmin axes. The degree of anisotropy (Pj) generally decreases towards a thrust or kinkzone (Fig. 3c). Furthermore, the shape of anisotropy is oblate for most of the samples away from a thrust or kinkzone, whereas in the vicinity of a such structure both prolate and oblate shapes are observed (Fig. 3c).

3.3.2 *Magnetic fabric at thrust surfaces*

An evolution of magnetic fabric for thrusts can be recognized in the models. The thrusts from the models show different amounts of displacement and therefore the observed magnetic fabric at each thrust can be related to the different degree of thrust maturity (Figs. 2, and 4). The kinks in front of the pop-up structure in Model A are described as an early stage of thrust development and samples from the kinks show vertical k_{min} axis distribution with horizontal k_{max} and k_{int} axes. The principal axes orientation of the kinks is similar to the principal axes orientation observed in samples away from the thrusts or kinkzones (Fig. 4a). Nevertheless, samples from the kinks show a lower degree of anisotropy (Pj) with some tendency towards a prolate fabric, which is different compared to samples away from thrusts and kinkzones (Figs. 3c, 5a, and 5d). The principal axes for samples from the forethrust (FT2) in the foreland of Model B are less clustered, as observed for the kinks in Model A (Fig. 4a). Additionally, at FT2, k_{max} and k_{int} create a magnetic foliation that is subhorizontal (dipping 10-20°) and are therefore not as horizontal as observed for samples away from the thrusts, but also not parallel to the thrust surface. k_{min} axes clusters tightly around the mean, with a steep inclination (˜80°) that verges slightly to the south-west (Fig. 4a). The degree of anisotropy for samples taken at FT2 is generally lower than for data collected at the kinks in the foreland of Model A. However, the peaks of the distribution of the degree of anisotropy for data from FT2 and the kinks in Model A are similar (Fig. 5d). The forethrust (FT) of Model C as well as the splayed forethrust (FT1) of Model B developed a magnetic foliation that converges into the orientation of the thrusts (Fig. 4a). For both forethrusts, most of the principal axes developed a subhorizontal magnetic foliation (i.e., girdle distribution of k_{max} and k_{int}) that tends into parallelism with the forethrusts and k_{min} axes started to rotate from vertical towards gentler inclinations in the south (Fig. 4a). Additionally, the degree of anisotropy at both forethrusts (FT and FT1) is comparable and is lower than observed for the kinks in Model A and FT2 in Model B (Fig. 5).

Along the backthrusts of all three models, k_{max} and k_{int} develop a magnetic foliation parallel to the thrust surfaces with k_{min} clustering at the pole (Fig. 4b). However, some principal axes deviate from this general alignment and clustering, which can be attributed to the local structural complexity and splaying of the backthrusts. Along the backthrust of Model B, a clustering of k_{max} indicate a clustering of magnetic lineation (k_{max}) parallel to the north-south shortening direction (Fig. 4b). In all thrusts (fore- and backthrusts) of the three models, a decrease in the degree of anisotropy can be observed downwards along the thrust surfaces, i.e., Pj decreases with depth for each thrust (Fig. 4d). Despite that the thrusts show different amount of displacement (Fig. 2), degree of anisotropy is still comparable between all thrusts (1.1 [?] Pj [?] 1.4), except for the kinks (early-stage thrusts) in the foreland of Model A, which have slightly higher degree of anisotropy (1.15 [?] Pj [?] 1.5) (Fig. 5). At depth, where thrusts are intersecting, slightly higher degree of anisotropy are observed. For example, at 8 – 13 cm depth interval of the backthrust in Model C, the forekink zones are intersecting with the backthrust and a slightly higher degree of anisotropy is calculated (Fig. 5). The shape of anisotropy at the thrusts is classified as a mix between prolate and oblate shapes (Fig. 3c). Nevertheless, the oblate shapes dominate at the thrusts (Fig. 3c).

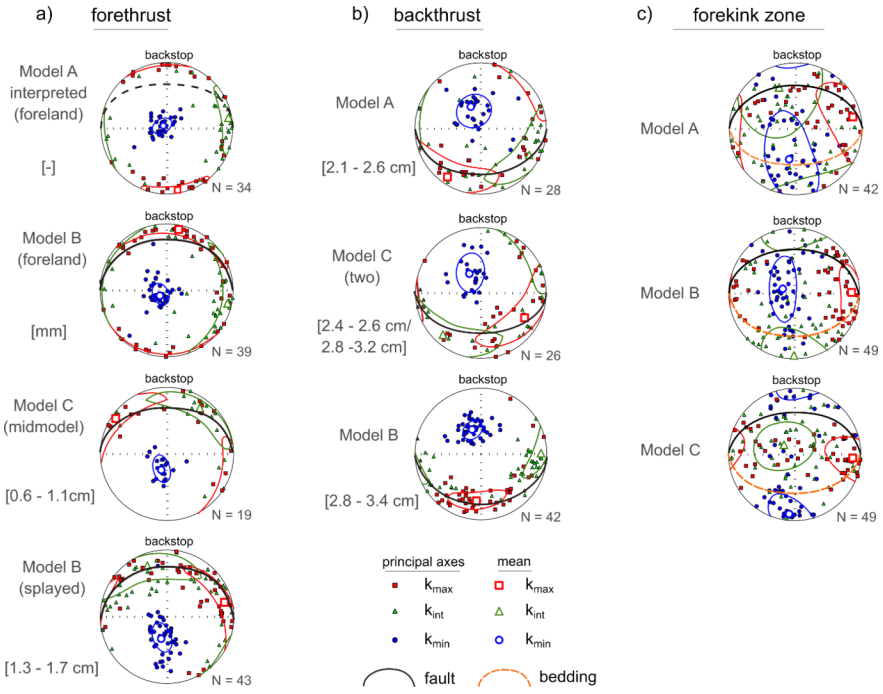

Figure 4: Equal-area projections showing principal axes of magnetic susceptibility with their means and 95 % confidence ellipses of the means (ellipses with same color as principal axes) from a) the forethrusts, b) backthrusts, and from c) the forekink zones from the three models A, B, and C with backstop to the North. The numbers in the brackets are the ranges in displacement along each thrust.

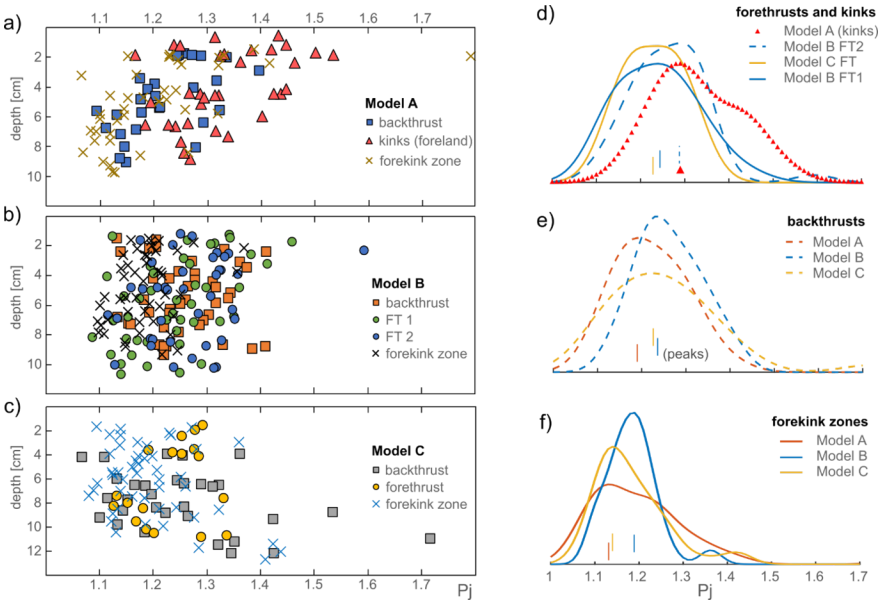

Figure 5: Distribution of degree of anisotropy (Pj) with depth for a) Model A, b) Model B, and c) Model C. The density of distribution probabilities, calculated with a Kernel distribution function, of the degree of anisotropy for each structure from the models are given in d) for forethrusts and foreland kinks, e)

backthrusts, and f) forekink zones. The position of the peak values (maxima) of each curve in d,e, and f are plotted with short vertical lines in the same color along the x-axis.

3.3.3 *Magnetic fabric in forekink zone*

The magnetic fabric within the relatively broad forekink zones can be summarized by principal axes spreading along north-south and east-west oriented great circle girdles (Fig. 4c). The forekink zone in Model A developed a scattered broad k_{max}-k_{int}girdle (i.e., magnetic foliation) dipping to the north with a subhorizontal mean of k_{max} towards east and a mean of k_{int} that is dipping ˜35° to the north. In contrast, k_{min} scatters as a broad north-south girdle with inclinations that vary from vertical to horizontal. Nevertheless, the mean of k_{min} is directed towards the south with an inclination of 52°, although with a very large mean confidence ellipse (Fig. 4c). By comparison, in the forekink zone of Model B, k_{min} developed a broad north-south girdle distribution as well, but with a narrower confidence ellipse and a mean clustering of k_{min} that is almost vertical (Fig. 4c). Furthermore, in the forekink zone of Model B, k_{max} is mainly clustering along an east and west axis, defining a magnetic lineation perpendicular to the shortening direction. The k_{int} axes of the forekink zone in Model B rotated into the north-south girdle distribution of k_{min} with a horizontal k_{int} mean axis aligned north-south. The two forekink zones in Model C developed a general principal axes distribution that can be compared to the magnetic fabric in the forekink zone of Model A (Fig. 4c). In the two forekink zones of Model C, $k_{max}$and k_{int} define a magnetic foliation trending perpendicular to the shortening direction with different inclinations but mainly with a vertical k_{int} mean and a suhorizontal east-west k_{max} mean. The k_{min} axes cluster subhorizontally in the two forekink zones of Model C with a north-south direction with a mean k_{min} plunging subhorizontally towards the south in the lower hemisphere projection (Fig. 4c). Notably, the minor forekink zone in the foreland of Model C (FKZ3) developed a similar AMS pattern as seen in the major forekink zones in this model (i.e., FKZ1 and 2). Overall, the shape anisotropy observed in forekink zones from all the three models are heterogeneous and range from oblate to prolate. The degree of anisotropy is comparable between the forekink zones of all three models and range from 1.05 [?]Pj [?] 1.35, which are the lowest ranges observed in this study (Fig. 5f). However, the peak of the distribution of the degree of anisotropy of the kinkzone in Model B is higher than the peaks for the forekink zones of Model A and Model C. (Fig. 5f).

4 Discussion

4.1 Strain distribution across the models

Of the three components of shortening (LPS, folding, and thrusting), LPS is dominant at the early stage of model deformation, leading to compaction of the shortened layers until folds and thrusts accommodate the shortening resulting in formation of an imbricate (Mulugeta and Koyi, 1992, Koyi, 1995, Koyi et al., 2003). This is also illustrated by our models, where the amount of LPS increases with bulk shortening but with a gradual decrease in strain accommodation giving way to an increase in faulting and folding as the imbricate is uplifted along the backthrust(s). Displacement of layers by faulting and folding are visible components of deformation during model shortening and localizes at certain zones within the models. Nevertheless, LPS, which is accommodated by grain rotation and repacking (Fig. 2), is not easy to identify by naked eye. Processes like compaction, grain rearrangement and grain reorientation contribute to the overall LPS and are consequences of stress propagation through the model (Koyi et al., 2003). However, since AMS monitors grain orientation and alignment, it can be used to indirectly deduce the degree of compaction and hence penetrative strain distribution. Reworking of the magnetic fabric due to an increase in LPS, folding and thrusting is typical for FTBs (e.g., Averbuch et al., 1992; Borradaile and Henry, 1997; Bakhtari et al., 1998; Saint-Bezar et al., 2002; Burmeister et al., 2009) and is a process that is observed in the three models presented in this study. All three models are shortened to different amount of bulk shortening, but express similar distribution of principal axes of magnetic susceptibility, degree of anisotropy (Pj) and shape of anisotropy (T). In general, there is a distinct difference between a magnetic fabric that developed away from a thrust or kinkzone to that within a thrust or kinkzone (Figs. 3 and 4). Consequently, the AMS data show (i) a change in the magnetic fabric as a function of distance to a thrust or kinkzone (Figs. 3a and 3c), and (ii) clear tectonic overprinting of a pre-existing magnetic fabric at faults and kinkzones.

4.1.1 *Compaction and folding in areas away from thrust and kinkzone*

Areas away from thrusts and kinkzones show a magnetic fabric that can be classified as a mixture between the initial fabric and tectonic fabric, where the tectonic fabric is represented by mainly LPS. The initial fabric is determined by model preparation as scraping produced an alignment of a magnetic lineation parallel to the shortening direction with k_{min} vertical to bedding (Almqvist and Koyi, 2018; Schofisch et al., 2021). This initial fabric is preserved in some places, regardless of distance to a thrust or kinkzone (Fig. 3b). However, a variation in principal axes distribution is illustrated by the distribution of k_{max} and k_{int} axes around the primitive circle with horizontal to subhorizontal (˜10-20deg dipping) inclinations (Fig. 3b). The change in magnetic fabric in the areas away from thrusts and kinkzones can be attributed to mainly penetrative strain, i.e., LPS (Fig. 2a). This agrees with observations of the penetrative-strain induced fabric from other modelling studies (Almqvist and Koyi, 2018; Schofisch et al. (2021) and natural examples (Kissel et al., 1986; Lee et al., 1990; Averbuch et al., 1992; Bakhtari et al., 1998; Pares and van der Plujim, 2002; Sans et al., 2003) where k_{max} is aligned perpendicular to the shortening direction and k_{min}remained vertical (pole to bedding). However, also gentle folding can be interpreted in the areas away from thrusts and kinkzones as bedding changes slightly along profile (Fig. 2). Folding is responsible for the change in inclination of the magnetic foliation, as $k_{max}$and k_{int} remain parallel to bedding, which has been reported by Averbuch et al. (1992) and Saint-Bezar et al. (2002). Consequently, the grain reorientation in areas away from thrusts and kinkzones, as described by the magnetic fabric, is characterized by tectonic compaction and folding. However, folding, i.e., bedding rotation in the areas away from thrusts and kinkzones, is very gentle and responsible for only few degrees, up to maximum 10deg, of inclination change of magnetic foliation.

Despite the variation in orientation of the principal axis, the degree of anisotropy for samples away from thrust and kinkzone illustrate a broad range of values (1.1 [?] *Pj* [?] 1.6). In the vicinity of a thrust or kinkzone prolate shape of anisotropy is recognizable, even though the overall fabric is oblate (Fig. 3c). This heterogeneous distribution in orientations of principal axes, degree of anisotropy and shape of ellipsoids (Fig. 3) describe a varying strain in the areas away from thrusts and kinkzones. This is known from observing deformation within an imbricate before fault initiation with optical methods (Adam et al., 2005; Dotare et al., 2016). Adam et al. (2005) described the strain distribution within an imbricate as "diffuse shear strain", whereas Dotare et al. (2016) recognized this "diffuse strain" as an accumulation of several short-lived weak shear bands during compaction of an imbricate. Our model results reveal a further detailed insight into the strain distribution in imbricates, especially, as the AMS data from the models show gradients in change of the magnetic fabric towards a thrust and a kinkzone.

4.1.2 S*train gradient towards thrusts and kinkzones*

Even though the principal axis distribution, degree of anisotropy and shape of anisotropy are scattered and described as a kind of "diffuse strain" in areas away from thrusts and kinkzones, a gradient in these magnetic fabric parameters can be described as a function of the distance to a thrust or kinkzone. With decreasing distance to a thrust or kinkzone, the variation of principal axis inclination increases, and a higher variation of principal axes orientations can be found closer to the thrust or kinkzone (Fig. 3a). Furthermore, a trend of decreasing degree of anisotropy is observed towards a thrust or kinkzone and the presence of prolate fabric increases in areas closer to a fault (Fig. 3c). Similar observations in changes of the magnetic fabric towards a thrust are identified from, for example, the French Alps (Kligfield et al., 1981), Corbieres in the Pyrenees (Averbuch et al. 1992), Central Appalachian FTB (Hirt et al., 2004), Gavarnie thrust in the Pyrenees (Marcen et al., 2018), the Barbados Accretionary Prism (Housen et al., 1996), and the Hikurangi Subduction Margin in New Zealand (Greve et al., 2020). Note that the first four studies above show an effect of magnetic mineral reprecipitation, and the latter two studies show an additional effect of fluids on the magnetic fabric. However, observations are similar to what our models show, and there is a compatible decreasing trend in the degree of anisotropy and alignment of magnetic grains towards the faults. Irrespective of the influence of fluids and mineral recrystallisation, our models suggest that brittle deformation plays a major role in reorientation of grains, and changes in magnetic fabric due to tectonic compaction and folding are important mechanisms towards a thrust.

Bulk shortening and hence the amount of deformation in a model, are reflected in the trends and gradients of the magnetic fabric change towards a thrust or kinkzone. With larger bulk shortening, more faults and kinkzones formed in the models, and displacement increased along the structures bounding the main boxfold, i.e., backthrusts and forekink zones. It appears, that with increasing shortening within a model, changes in magnetic fabric between a thrust-induced fabric and magnetic fabric away from thrusts and kinkzones are more distinct. The increase in variety of inclination of the principal axes with decreasing distance to a thrust or kinkzone occurs over smaller distances (Fig. 3a). For example, the largest amount of strain is accommodated in Model C (Fig. 2f), and the change in principal axes inclination as a function of distance to thrust and kinkzone is observed for a smaller distance in this model compared to models A and B, where the gradient is steeper, more linear and is observed over a longer distance (Fig. 3a). Also, the degree of anisotropy shows less scattering and a clearer decrease in Model C (Fig. 3c), which is not a consequence of the differing number of samples between the models (Table 1). Consequently, the transition of a magnetic fabric away from a thrust or kinkzone towards a magnetic fabric at a thrust or kinkzone is defined by the amount of bulk shortening, which is also reflected in the amount of displacement along a thrust.

Furthermore, most studies interpret an increase in strain, especially LPS, from the foreland to the hinterland in FTBs over a larger regional scale. However, such increase in strain as a function of distance to the hinterland is not linear and it has been observed that accumulation of strain is rather expressed by localized minor faults and deformation zones that accretion towards the hinterland (e.g., Groshong et. al. 1984, Averbuch et al., 1992; Dittmar et al., 1994). However, our models show that strain is also changing and increasing within imbricates, towards its boundaries on a local scale. Consequently, AMS provides useful insights into the strain distribution of an imbricate and therefore the model results encourage studying strain distribution of natural analogues within FTBs at local scales.

4.1.3 *Tectonic overprinting by thrusting*

The magnetic fabric observed at a thrust is distinct from the other sets of magnetic fabric observed in the other areas of the models. Moreover, greatest change in magnetic fabric from the initial fabric is observed at a thrust, especially where the displacements by thrusts are large. Thrusts from all three models, i.e., backthrusts and forethrusts, created a similar fabric pattern that reflects the geometry of the thrusts, as the magnetic foliation (k_{max}-k_{int} girdle) is scattered, generally along a great circle parallel to the thrust plane, instead of being parallel to the bedding (Figs. 4a and b). Consequently, thrusting has a significant impact on the development of the magnetic fabric and such fabric can be described as "thrust-induced fabric" (Schofisch et al. 2021). Samples from a thrust show a higher variation in the shape of anisotropy with both oblate and prolate shape anisotropy. Compared to LPS-produced fabric in areas away from the thrust, more prolate shapes can be observed with a general lower degree of anisotropy in thrusts (Fig. 3c). The change from oblate to a more prolate fabric with a lower degree in anisotropy is consistently observed in the vicinity of a thrusts in the models and is common in nature as deformation increases and localizes towards a structure (Kligfield et al., 1981; Hirt et al., 2004). In general, changes in magnetic fabric, with magnetic foliation parallel to thrust surface and low degrees of anisotropy, are in agreement with experiments (Borradaile and Alford, 1988; Borradaile and Puumala,1989; Housen et al., 1993; Schofisch et al., 2021), numerical models (Housen et al., 1993), and field observations (e.g., Averbuch, et al. 1992; Housen et al., 1996; Pares and van der Pluijm, 2002; 2004; Hirt et al., 2004; Marcen et al., 2018; Greve et al., 2020).

AMS analysis show that prominent changes in the degree of anisotropy and alignment of principal axes can be observed at the onset of thrusting (Figs. 4 and 5). The kinks at the front of the main boxfold in Model A and the forethrust in Model B with a minor offset show a mixture between the magnetic fabric observed farther away from the thrust and at more mature thrusts, with larger displacement like the backthrusts (Figs. 3 and 4). Compaction precedes thrusting (e.g., Adam et al., 2005; Dotare et al., 2016) and further kinking takes place before the sand layers are offset by thrusting. Therefore, thrusting will overprint a LPS-affected fabric, that has also a signature of folding. The kinks in Model A and the forethrust in Model B illustrate a transition from a "compactional fabric" to a "thrust-induced fabric", which occurs with kink initiation and minimal layer offset in our models. This means that compaction, kinking and folding are the main

components responsible for principal axes reorientation prior to thrusting.

With larger displacement along a thrust, a "thrust-induced fabric" shows a general alignment of magnetic foliation with the thrust surface. This thrust-induced fabric is seen in the well-developed fore- and backthrusts of all three models (Figs. 3a and b). Especially at the backthrusts, overprinting of a compacted and folded magnetic fabric is more efficient, as deformation within the zone of thrust initiation created alignment of principal axes with the thrust surface (Fig. 3b). Nevertheless, variations in principal axis orientation can occur due to structural complexity, for example, where a fore- and backthrust are intersecting (Model C), or where a splay developed (Model B). Note that an increase of degree of anisotropy at lower levels in the models is related to the intersection of other thrusts (Fig. 5). For example, the backthrust of Model C is intersecting with the forekink zones at depth in the model and an influence on the magnetic fabric is expected in this area (Fig. 6).

As strain, especially LPS, is heterogenous throughout a model (Mulugeta and Koyi, 1992; Koyi, 1995), notably with depth (Koyi et al., 2003), the variation in strain will also be reflected in the magnetic fabric prior to thrusting and can be inherited in further overprinting (e.g., Pares and von der Pluijm, 2002; Ferre et al., 2014; Marcen et al., 2018). The models reported here also show a change in strain with depth (Figs. 2d, e, and f), especially by decreasing displacement along the thrusts (Fig. 2). The changes in displacement and strain accommodation with depth in the models can explain a general decreasing trend in the degree of anisotropy downwards the thrusts (Fig. 5). Relatively higher values in degree of anisotropy reveal a preferred alignment of the magnetic grains within the samples, whereas lower degrees show less preferred alignment of grains (e.g., Borradaile and Jackson, 2010; Pares, 2015). This means that thrusting was less efficient in realigning the grains at depth, and an AMS signal prior to thrusting is inherited in the final modelled magnetic fabric. A similar observation is made at the Gavarnie thrust in the Pyrenees (Marcen et al., 2018), where an intersection lineation prior the Alpine deformation is inherited during reactivation of the thrust and a low degree of anisotropy is observed at the reworked Variscan fabric.

Additionally, the trend of decreasing degree of anisotropy with depth along a thrust seems to be independent of the amount of displacement at a thrust, as the same trend can be interpreted at each thrust from the three models, whereas each thrust differs in amount of displacement. The changes in AMS signal at a thrust needs to be discussed considering relative changes in deformation along an individual thrust instead of comparing absolute numbers of displacement for each thrust. Larger displacement, which is observed in upper segments of the thrusts, produce higher degree of anisotropy and therefore grains are more aligned compared to deeper segments of the thrusts, where lower displacements and lower degree of anisotropy are observed. However, comparing data between different segments of different thrusts, but with similar amount displacement, is deceiving, because different segments of thrusts and, in general, thrusts from different models have different deformation histories in general.

The trend of decreasing degree of anisotropy with depth at a thrust is less obvious for thrusts in Model B and C compared to thrusts in Model A (Figs. 5a, b, and c). This further emphasizes that strong changes in magnetic fabric are observed at the beginning of thrust initiation, as the thrusts in Model A are less mature compared to the thrusts from the other models. With increasing deformation and further displacement at a thrust, differences in magnetic fabric (e.g., inclination of principal axes or degree of anisotropy) between upper and lower parts of a thrust will decrease. Our models are limited to grain reorientation only and therefore, alignment of principal axes of susceptibility parallel to a thrust will reach a certain degree of anisotropy. However, AMS data from the modelled thrusts reveal "heterogeneous strain" along thrusts and shear zones, which are typical observations in nature (e.g., Ferre et al., 2014). Consequently, this highlights the importance of brittle reorientation of grains during thrust development.

4.1.4 *The internal deformation of kinkzones*

The initial model setup and the amount of bulk shortening are reflected in the evolution of the model and, especially, in the creation of the forekink zones. The geometric variation in width and extent of the forekink zones from the different models, are also expressed in the magnetic fabric for each forekink zone. The forekink

zones consist of rotated bedding parallel to the backthrust and many forethrusts with small displacement (Fig. 2). The small displacement (millimeters) within the kinkzone is significant enough to rotate grains, which results in a broad spread of the principal axes of susceptibility (Fig. 4c). Overall, the magnetic fabric in the forekink zones can be described by an interplay among LPS, thrusting, and folding, while folding includes bedding rotation parallel to the backthrust on a larger scale and internal kinking due to forethrust creation on a smaller scale. The different mechanisms of deformation contributed differently in each kinkzone and can be revealed by the magnetic fabric. The kinkzone fabric from all three models, especially the means of the principal axes of susceptibility and their confidence ellipses, are comparable and summarized by a mean of k_{max} oriented to the East-West and by means of k_{min} and k_{int} within a broad north-south girdle (Fig. 4c). The k_{max} clustering defines a magnetic lineation normal to the shortening direction and parallel to the fold axis of the minor kinks and bedding-thrust intersection within all models. However, the principal axes are rather scattered, which is also reflected by the appearance of low degree of anisotropy, which is even lower than observed at thrusts or in areas away from thrust and kinkzone (Fig. 5). Low degree of anisotropy derives from the intersection of folding and thrusting, without a dominance of either of these deformation processes. This agrees with natural examples, where S-C-structures are producing a low degree of anisotropy (Ferre et al., 2014; Marcen et al., 2018). However, the composite magnetic fabric needs to be analyzed carefully, because summarizing different grain orientations in a bulk susceptibility makes AMS to strain correlation more difficult (Housen et al., 1993; Ferre et al., 2014). In contrast, at the intersection between backthrust and forekink zone, e.g., in Model C, the intersection is well defined and produces a relatively higher degree of anisotropy compared to the interplay of thrusting and folding in the kinkzones itself.

As bedding within the forekink zone is generally parallel to the backthrust, the magnetic fabric depicts this bedding rotation. Several previous studies have shown that the magnetic foliation remains parallel to the bedding during folding (Averbuch et al., 1992; Bakhtari et al., 1998; Saint-Bezar et al., 2002). However, the models presented in this study show that several minor forethrusts are developed within a forekink zone. Consequently, the fabric in these forekink zones is not only the product of bedding rotation, but the effect of thrusting needs to be considered too. In a steep forekink zone inclination, which cause larger throw, thrusting within the kinkzone will have a greater impact on AMS signature, as seen in Model A by the development of broad gridle of k_{max} and k_{int} subparallel to the fault surface (Figs. 2 and 4c). An even clearer magnetic foliation and clustering of k_{min} (seen by narrower confidence ellipses compared to forekink zone in Model A) is observed in the forekink zones of Model C (Fig. 4c). However, in the kinkzones of Model C, the magnetic foliation does not align with the forethrust and is rather parallel to the intersection lineation of bedding and forethrusts of the forekink zone. Nevertheless, k_{min} distribution of the kinkzones in Model A and C are clustering to the pole of the forethrusts within the kinkzones. AMS data from the forekink zone in Model B create compatible narrow confidence ellipses as the forekink zones in Model C, but here the position of k_{min} and $k_{int}$are swapped (Fig. 4c). Obvious step-like kinks developed in the forekink zone in Model B (Fig. 2b), which are less visible in the other models. Consequently, additional internal folding needs to be discussed for the forekink zone of Model B, which explains, that k_{min} is rather distributed in a girdle as poles to the internal folds instead of clustering perpendicular to the thrust surface. However, k_{max} lineation is still parallel to the intersection of the forethrusts and bedding in the forekink zone of Model B, as observed in all forekink zones of all models. Generally, the magnetic fabric highlights the influence of different deformation processes within a kinkzone and reveals strain in more detail.

The observation that the "kinkzone fabric" in the models is a consequence of an interplay between folding and faulting is similar to the observation of Greve et al. (2020). In Greve et al. (2020), the zone right above the major fault zone, called the 'mid hangingwall' in their study, is pervaded by thrusts and has steep bedding. The analyzed AMS fabric from this zone is very similar to the "kinkzone fabric" in our models, where k_{max} clusters perpendicular and a k_{int}-k_{min} girdle is defined parallel to the shortening direction. Another comparison can be done with observations from the shear zone at the Gavarnie thrust in the Pyrenees (Marcen et al., 2018). S-C-structures create a composite magnetic fabric producing magnetic lineation parallel to the intersection of S- and C-planes. Similar magnetic lineation is produced in our case by the intersection of

folding and thrusting. In general, it is known from natural examples, that the intersection of bedding and cleavage in a deformed rock creates a magnetic lineation parallel to it (e.g., Borradaile and Tarling, 1981; Kligfield et al., 1981; Pares and van der Pluijm, 2002; Hirt et al., 2004). However, competing fabric within in one AMS sample lead to a composite fabric, that may not reflect the strain within the deformation zone (Housen, 1993; Ferre et al., 2014). Nevertheless, AMS data from the modelled kinkzones can be associated to different accommodation of deformation within the kink zone as described above. Consequently, AMS reveals different contributions to strain within the kinkzone and vice versa, different deformation processes within a kinkzone lead to complex sets of heterogenous kinkzone fabric.

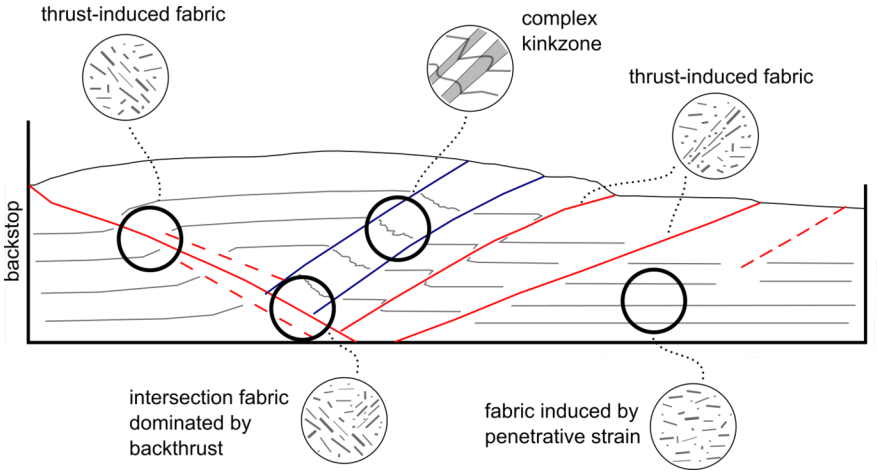

Figure 6: Schematic sketch of grain alignment in the models.

5 Conclusions

Measurements of the magnetic fabric in three different shortened analogue models describe strain distribution across a thrust imbricate, i.e., pop-up structure with associated thrusts and kinkzones. The AMS data reflect a strain gradient from (i) an initial to compactional magnetic fabric towards a (ii) thrust-induced fabric or (iii) composite fabric within forekink zones (Fig. 6). Generally, the geometry of a thrust determines the alignment of the magnetic fabric shown by clustering and girdle distribution of the principal axes. In contrast, folded layers displaced by minor thrusts display a more complicated AMS pattern within the kinkzones. However, fabric analysis in the kinkzones indicates the importance of strain accommodation of different deformation mechanism like thrusting or folding. In addition, at thrusts, AMS signatures from deformation prior thrusting can be inherited in the finite magnetic fabric, which explains a varying strain distribution and interpretation along thrusts in general. Overall, this AMS study outlines strain distribution and magnitude within different parts of an imbricate in more detail. Strain is changing as function of distance towards localized deformation zones (e.g., thrusts and kinkzones) and with larger bulk shortening, the change in strain between areas away and within deformation zones is more distinct.

Acknowledgement This study is supported by a research grant from the Swedish Research Council to HK and BA (VR 2017-04519). The authors acknowledge LKAB Minerals Luleå (Sweden) for providing the magnetite for modelling. We thank the editor for editorial handling, and anonymous reviewers for constructive comments. There are no conflicts of interest.

Data Availability StatementAMS data from the three models of this study will be available at doi:10.17632/zs7n4t57k4.1, an open-source online data repository hosted at Mendeley Data (Schöfisch, 2021). Additionally, uncommented plots illustrating magnetic fabric distribution in the models can be found in the supporting information (Figures S1-S8).

References

Adam, J., Urai, J. L., Wieneke, B., Oncken, O., Pfeiffer, K., Kukowski, N., et al. (2005). Shear localisation and strain distribution during tectonic faulting - New insights from granular-flow experiments and high-resolution optical image correlation techniques. Journal of Structural Geology, 27(2), 283–301. https://doi.org/10.1016/j.jsg.2004.08.008

Almqvist, B. S. G., & Koyi, H. (2018). Bulk strain in orogenic wedges based on insights from magnetic fabrics in sandbox models. Geology, 46(6), 483–486. https://doi.org/10.1130/G39998.1

Averbuch, O., Frizon de Lamotte, D., & Kissel, C. (1992). Magnetic fabric as a structural indicator of the deformation path within a fold-thrust structure: a test case from the Corbières (NE Pyrenees, France). Journal of Structural Geology, 14(4), 461–474. https://doi.org/10.1016/0191-8141(92)90106-7

Bakhtari, H. R. ., Frizon de Lamotte, D. ., Aubourg, C. ., & Hassanzadeh, J. . (1998). Magnetic fabrics of Tertiary sandstones from the Arc of Fars (Eastern Zagros, Iran). Tectonophysics, 284, 299–316. https://doi.org/PIIS0040-1951(97)00179-0

Borradaile, G. J., & Puumala, M. A. (1989). Synthetic magnetic fabrics in a plasticene medium. Tectonophysics, 164(1), 73–78. https://doi.org/10.1016/0040-1951(89)90235-7

Borradaile, G.J., & Henry, B. (1997). Tectonic applications of magnetic susceptibility and its anisotropy. Earth-Science Reviews, 42(1–2), 49–93. https://doi.org/10.1016/S0012-8252(96)00044-X

Borradaile, G J, & Alford, C. (1988). Experimental shear zones and magnetic fabrics. Journal of Structural Geology, 10(8), 895–904.

Borradaile, Graham J., & Jackson, M. (2010). Structural geology, petrofabrics and magnetic fabrics (AMS, AARM, AIRM). Journal of Structural Geology, 32(10), 1519–1551. https://doi.org/10.1016/J.JSG.2009.09.006

Borradaile, Graham J., & Tarling, D. H. (1981). The influence of deformation mechanisms on magnetic fabrics in weakly deformed rocks. Tectonophysics, 77(1–2), 151–168. https://doi.org/10.1016/0040-1951(81)90165-7

Burmeister, K. C., Harrison, M. J., Marshak, S., Ferré, E. C., Bannister, R. A., & Kodama, K. P. (2009). Comparison of Fry strain ellipse and AMS ellipsoid trends to tectonic fabric trends in very low-strain sandstone of the Appalachian fold-thrust belt. Journal of Structural Geology, 31(9), 1028–1038. https://doi.org/10.1016/j.jsg.2009.03.010

Dahlen, F. A., Suppe, J., & Davis, D. (1984). Mechanics of Fold-and-Thrust Belts and Accretionary Wedges: Cohesive Coulomb Theory. Journal of Geophysical Research, 89(B12), 10087–10101. https://doi.org/10.1029/JB089iB12p10087

Davis, D., Suppe, J., & Dahlen, F. A. (1983). Mechanics of fold-and- thrust belts and accretionary wedges. Journal of Geophysical Research, 88(B2), 1153–1172. https://doi.org/10.1029/JB088iB02p01153

Dittmar, D., Meyer, W., Oncken, O., Schievenbusch, T., Walter, R., & von Winterfeld, C. (1994). Strain partitioning across a fold and thrust belt: the Rhenish Massif, Mid-European Variscides. Journal of Structural Geology, 16(10), 1335–1352. https://doi.org/10.1016/0191-8141(94)90001-9

Dotare, T., Yamada, Y., Adam, J., Hori, T., & Sakaguchi, H. (2016). Initiation of a thrust fault revealed by analog experiments. Tectonophysics, 684, 148–156. https://doi.org/10.1016/j.tecto.2015.12.023

Ferré, E. C., Gébelin, A., Till, J. L., Sassier, C., & Burmeister, K. C. (2014). Deformation and magnetic fabrics in ductile shear zones: A review. Tectonophysics, 629(C), 179–188. https://doi.org/10.1016/j.tecto.2014.04.008

Graham, J. W. (1966). Significance of Magnetic Anisotropy in Appalachian Sedimentary Rocks. In The Earth Beneath the Continents: A Volume of Geophysical Studies in Honor of Merle A. Tuve. (1966), Geophys. Monogr. Ser., vol. 10, edited by J. S. Steinhart and T. J. Smith, pp. 627-648, AGU, Washington, D. C. (pp. 627–648). https://doi.org/10.1029/GM010p0627

Graveleau, F., Malavieille, J., & Dominguez, S. (2012). Experimental modelling of orogenic wedges: A review. Tectonophysics, 538–540, 1–66. https://doi.org/10.1016/j.tecto.2012.01.027

Greve, A., Kars, M., Zerbst, L., Stipp, M., & Hashimoto, Y. (2020). Strain partitioning across a subduction thrust fault near the deformation front of the Hikurangi subduction margin, New Zealand: A magnetic fabric study on IODP Expedition 375 Site U1518. Earth and Planetary Science Letters, 542, 116322. https://doi.org/10.1016/j.epsl.2020.116322

Groshong, R. H., Pfiffner, A., & Pringle, L. R. (1984). Strain partitioning in the Helvetic thrust belt of eastern Switzerland from the leading edge to internal zone. Journal of Structural Geology, 6(1), 5–18.

Groshong, Richard H. (2019). Area-constant strain and dilation in sandbox models: Insights from whole-model area balance. Journal of Structural Geology, 118(November 2018), 279–283. https://doi.org/10.1016/j.jsg.2018.11.003

Gutscher, M. A., Kukowski, N., Malavieille, J., & Lallemand, S. (1996). Cyclical behavior of thrust wedges: Insights from high basal friction sandbox experiments. Geology, 24(2), 135–138. https://doi.org/10.1130/0091-7613(1996)024<0135:CBOTWI>2.3.CO;2

Hirt, A. M., Lowrie, W., Lüneburg, C., Lebit, H., & Engelder, T. (2004). Magnetic and mineral fabric development in the ordovician Martinsburg Formation in the Central Appalachian Fold and Thrust Belt, Pennsylvania. Geological Society Special Publication, 238(1995), 109–126. https://doi.org/10.1144/GSL.SP.2004.238.01.09

Housen, B. A., Richter, C., & van der Pluijm, B. A. (1993). Composite magnetic anisotropy fabrics: experiments, numerical models and implications for the quantification of rock fabrics. Tectonophysics, 220(1–4), 1–12. https://doi.org/10.1016/0040-1951(93)90219-A

Housen, B. A., Tobin, H. J., Labaume, P., Leitch, E. C., Maltman, A. J., Shipley, T., et al. (1996). Strain decoupling across the decollement of the Barbados accretionary prism. Geology, 24(2), 127–130. https://doi.org/10.1130/0091-7613(1996)024<0127:SDATDO>2.3.CO;2

Hrouda, F. (1982). Magnetic anisotropy of rocks and its application in geology and geophysics. Geophysical Surveys, 5(1), 37–82. https://doi.org/10.1007/BF01450244

Huiqi, L., McClay, K. R., & Powell, D. (1992). Physical models of thrust wedges. In Thrust Tectonics. https://doi.org/10.1007/978-94-011-3066-0_6

Jelinek, V. (1981). Characterization of the magnetic fabric of rocks. Tectonophysics, 79(3–4), T63–T67. https://doi.org/10.1016/0040-1951(81)90110-4

Kissel, C., Barrier, E., Laj, C., & Lee, T. -Q. (1986). Magnetic fabric in "undeformed" marine clays from compressional zones. Tectonics, 5(5), 769–781. https://doi.org/10.1029/TC005i005p00769

Kligfield, R., Owens, W. H., & Lowrie, W. (1981). Magnetic susceptibility anisotropy, strain, and progressive deformation in Permian sediments from the Maritime Alps (France). Earth and Planetary Science Letters, 55(1), 181–189. https://doi.org/10.1016/0012-821X(81)90097-2

Koyi, H. (1997). Analogue modelling: From a qualitative to a quantitative technique - A historical outline. Journal of Petroleum Geology, 20(2), 223–238. https://doi.org/10.1111/j.1747-5457.1997.tb00774.x

Koyi, H. A., & Maillot, B. (2007). Tectonic thickening of hanging-wall units over a ramp. Journal of Structural Geology, 29(6), 924–932. https://doi.org/10.1016/j.jsg.2007.02.014

Koyi, H. A., Sans, M., Teixell, A., & Zeyen, H. (2003). The Significance of Penetrative Strain in the Restoration of Shortened Layers-Insights from Sand Models and the Spanish Pyrenees. Thrust Tectonics and Hydrocarbon Systems: AAPG Memoir., 82, 1–16. Retrieved from http://gent.uab.cat/ateixell/sites/gent.uab.cat.ateixell/files/16.-Koyietal03.pdf

Koyi, Hemin. (1995). Mode of internal deformation in sand wedges. Journal of Structural Geology, 17(2), 293–300. https://doi.org/10.1016/0191-8141(94)00050-A

Maillot, B., & Koyi, H. (2006). Thrust dip and thrust refraction in fault-bend folds: Analogue models and theoretical predictions. Journal of Structural Geology, 28(1), 36–49. https://doi.org/10.1016/j.jsg.2005.10.001

Maillot, B., & Leroy, Y. M. (2003). Optimal dip based on dissipation of back thrusts and hinges in fold-and-thrust belts. Journal of Geophysical Research: Solid Earth, 108(B6), 1–17. https://doi.org/10.1029/2002jb002199

Marcen, M., Casas-Sainz, A. M., Roman-Berdiel, T., Oliva-Urcia, B., Soto, R., & Aldega, L. (2018). Kinematics and strain distribution in an orogen-scale shear zone: Insights from structural analyses and magnetic fabrics in the Gavarnie thrust, Pyrenees. Journal of Structural Geology, 117(September), 105–123. https://doi.org/10.1016/j.jsg.2018.09.008

Mulugeta, G., & Koyi, H. (1992). Episodic accretion and strain partitioning in a model sand wedge. Tectonophysics, 202, 319–333. https://doi.org/10.1016/0040-1951(92)90117-O

Mulugeta, Genene. (1988). Modelling the geometry of Coulomb thrust wedges. Journal of Structural Geology, 10(8), 847–859. https://doi.org/10.1016/0191-8141(88)90099-5

Nilforoushan, F., Koyi, H. A., Swantesson, J. O. H., & Talbot, C. J. (2008). Effect of basal friction on surface and volumetric strain in models of convergent settings measured by laser scanner. Journal of Structural Geology, 30(3), 366–379. https://doi.org/10.1016/J.JSG.2007.09.013

Pares, J. M., & van der Pluijm, B. A. (2004). Correlating magnetic fabrics with finite strain: Comparing results from mudrocks in the Variscan and Appalachian Orogens. Geologica Acta, 2(3), 213–220. https://doi.org/10.1344/105.000001428

Pares, Josep M., & Van Der Pluijm, B. A. (2002). Evaluating magnetic lineations (AMS) in deformed rocks. Tectonophysics, 350(4), 283–298. https://doi.org/10.1016/S0040-1951(02)00119-1

Pares, Josep M., Van der Pluijm, B. A., & Dinares-Turell, J. (1999). Evolution of magnetic fabrics during incipient deformation of mudrocks (Pyrenees, northern Spain). Tectonophysics, 307(1–2), 1–14. https://doi.org/10.1016/S0040-1951(99)00115-8

Ramsay, J. G., & Huber, M. I. (1983). The techniques of modern structural geology. Volume 1: strain analysis. The Techniques of Modern Structural Geology. Volume 1: Strain Analysis. https://doi.org/10.1016/0040-1951(86)90091-0

Rochette, P., Jackson, M., & Aubourg, C. (1992). Rock Magnetism and the Interpretation of AMS, (92), 209–226.

Saint-Bezar, B., Hebert, R. L., Aubourg, C., Robion, P., Swennen, R., & Frizon De Lamotte, D. (2002). Magnetic fabric and petrographic investigation of hematite-bearing sandstones within ramp-related folds: Examples from the South Atlas Front (Morocco). Journal of Structural Geology, 24(9), 1507–1520. https://doi.org/10.1016/S0191-8141(01)00140-7

Sans, M., Verges, J., Gomis, E., Pares, J. M., Schiattarella, M., Trave, A., et al. (2003). Layer parallel shortening in salt-detached folds: Constraint on cross-section restoration. Tectonophysics, 372(1–2), 85–104. https://doi.org/10.1016/S0040-1951(03)00233-6

Schellart, W. P., & Strak, V. (2016). A review of analogue modelling of geodynamic processes: Approaches, scaling, materials and quantification, with an application to subduction experiments. Journal of Geodynamics, 100, 7–32. https://doi.org/10.1016/j.jog.2016.03.009

Schofisch, T., Koyi, H., & Almqvist, B. (2021). Influence of decollement friction on anisotropy of magnetic susceptibility in a fold-and-thrust belt model. Journal of Structural Geology, 144(September 2020).

https://doi.org/10.1016/j.jsg.2020.104274

Schofisch, Thorben (2021), "popupStructure_3AnalogModels_MagneticFabricDistr", Mendeley Data, v1 http://dx.doi.org/10.17632/zs7n4t57k4.1

Storti, F., Salvini, F., & McClay, K. (2000). Synchronous and velocity-partitioned thrusting and thrust polarity reversal in experimentally produced, doubly-vergent thrust wedges: Implications for natural orogens. Tectonics, 19(2), 378–396. https://doi.org/10.1029/1998TC001079

Suppe, J. (1983). Geometry and kinematics of fault-bend folding. American Journal of Science, 283(7), 684–721. https://doi.org/10.2475/ajs.283.7.684

Teh-Quei Lee, Kissel, C., Laj, C., Chorng-Shern Horng, & Yi-Teh Lue. (1990). Magnetic fabric analysis of the Plio-Pleistocene sedimentary formations of the Coastal Range of Taiwan. Earth and Planetary Science Letters, 98(1), 23–32. https://doi.org/10.1016/0012-821X(90)90085-C

Magnetic Fabric Signature within a Thrust Imbricate; an analogue modelling approach

T. Schöfisch[1], H. Koyi[1*] , and B. Almqvist[1]

[1]Hans Ramberg Tectonic Laboratory, Department of Earth Sciences, Uppsala University, Villavägen 16, 752 36 Uppsala, Sweden.

Corresponding author: Thorben Schöfisch (thorben.schofisch@geo.uu.se)

*current address: Department of Earth Sciences, Khalifa University of Science and Technology, Abu Dhabi, United Arab Emirates

Key Points:

- Anisotropy of magnetic susceptibility as strain indicator within three analogue models simulating a development of a pop-up structure
- Characteristic sets of magnetic fabric are developed for each structure in the models, which reveal deformation in more detail
- Gradients in changes in magnetic fabric are recognized as function of distance towards a thrust or kinkzone

Abstract

In this study, we report results from three analogue models with similar initial setup and different amounts of bulk shortening, to simulate a development of a pop-up structure in fold-and-thrust belts at different stages. Samples are taken in different places of the deformed models for analysis using anisotropy of magnetic susceptibility. Shortening of the models resulted in the formation of a pop-up structure, which is bounded by backthrust(s) and complex forekink zone(s). Several forethrusts at different degrees of maturity developed in front of the pop-up structure. Three distinct types of magnetic fabric can be identified throughout the models: (i) a compactional oblate fabric that changes as function of distance towards a localized deformation zone (e.g., thrust or kinkzone), (ii) a thrust-induced fabric with magnetic foliation parallel to the thrust surface, and (iii) a complex forekink zone fabric with broad girdle distributions of principal axes and magnetic lineation perpendicular to shortening direction. The latter indicate interplay between folding and thrusting of the shortened sand layers. Additionally, a decrease in degree of anisotropy with appearance of a quantitatively more prolate fabric can be observed towards the thrusts and kinkzones. Additionally at thrusts, a variation in strain is reflected by the magnetic fabric and can be inherited in a thrust-induced fabric. In conclusion, strain is changing as function of distance towards localized deformation zones with characteristic fabric, and differences in magnetic fabric are distinct between data away and within deformation zones as deformation zones mature.

Plain Language Summary

Deformation within fold-and-thrust belts occurs as thrusting (displacement along weak zones), folding (bending of rock units) and internal deformation.

The internal deformation, like compaction and grain realignment, is hard to analyze by the naked eye. Fortunately, the magnetic properties of grains can be measured and provide information of grain realignment within an imbricate. In this study, we combine analogue modelling with magnetic analysis to track the internal deformation of imbricates in detail. We modelled imbricates and analyzed the magnetic fabric within the models. Our observations show a gradual change in magnetic fabric within an imbricate towards thrusts and kinkzones, which bound the imbricate, showing increasing deformation. At the thrusts, the magnetic fabric aligns parallel to the thrust surface, whereas in the kinkzone a complex interplay between folding and thrusting is revealed. Our results can be compared to natural examples, as observation from models and published natural analogies are comparable. Our study provides insights into the strain distribution and gradients within imbricates.

1 Introduction

Three main components take up deformation in fold-and-thrust belts (FTBs); layer-parallel shortening (LPS), folding and faulting. In FTBs, most structures like thrusts and folds can be mapped and analyzed with different techniques by their optical appearance (e.g., Ramsay and Huber, 1983). However, in the absence of strain markers, penetrative strain (i.e., layer-parallel shortening), which is not always easy to quantify in the field, can also be quantified by focusing on an intrinsic property of the rocks, i.e., their magnetic susceptibility. The anisotropy of magnetic susceptibility (AMS) has proven to be a useful tool to study strain in different tectonic regimes and lithologies (e.g., Graham, 1966; Hrouda, 1982; Averbuch et al., 1992; Borradaile and Henry, 1997; Bakhtari et al., 1998; Saint-Bezar et al.,2002; Borradaile and Jackson, 2010; Ferré et al., 2014; Parés, 2015).

Quantifying penetrative strain in fold-thrust belts is not always possible due to lack of strain markers and outcrops and difficulty of accessing deeper levels. However, in analogue models, where initial and subsequent deformation stages are well documented and different parts are accessible, strain partitioning in model FTBs and accretionary wedges can be quantified, which assists in interpreting field observations and the development of FTBs (e.g., Davis et al., 1983; Dahlen et al., 1984; Mulugeta, 1988; Mulugeta and Koyi, 1992; Liu et al., 1992; Koyi, 1995; Gutscher et al., 1996; Storti et al., 2000; Koyi et al., 2003; Sans et al., 2003; Adam et al., 2005; Graveleau et al., 2012; Dotare et al., 2016). It has been reported that in most of the model studies simulating FTBs, the granular material (simulating sedimentary rocks) is compacted, and the deformation front propagates from the backstop towards the foreland of the model. Shear bands precede thrust initiation (Dotare et al., 2016) and with further shortening thrusts act as ramps (e.g., Suppe, 1983) where strain is refracted into the hangingwall (Maillot and Leroy, 2003; Maillot and Koyi, 2006; Koyi and Maillot, 2007). Imbricates between the thrusts deform internally (Koyi, 1995) and overall strain varies both with time and depth (Mulugeta and Koyi, 1992; Koyi et al., 2003). To monitor and quantify penetrative deformation in

analogue models, passive markers printed on the surface of the models are monitored by photogrammetry or laser scanning (reviews by Koyi, 1997; Graveleau et al., 2012; Schellart and Strak, 2016). LPS in models is estimated by cross-section balancing and area calculation (e.g., Koyi et al., 2003; Groshong, 2019), analysis of surface deformed strain markers and volumetric strain (Nilforoushan et al., 2008). Recently, AMS has also been introduced in analogue modelling to quantify strain in models simulating FTBs (Almqvist and Koyi, 2018). In FTBs, the evolution of the magnetic fabric depends on the amount of shortening and location within a FTB. With increasing strain, a primary fabric, i.e., sedimentary fabric, will be overprinted to a completely reoriented tectonic fabric. A mixture of magnetic fabric patterns between primary and tectonic fabric indicates an intermediate fabric, that results from a moderate tectonic overprint of the sedimentary fabric. Intermediate and tectonic magnetic fabric are typical in FTBs and paths in strain change described by tectonic overprint derive from field observations (e.g., Graham, 1966; Borradaile and Tarling, 1981; Kligfield et al., 1981; Averbuch et al., 1992; Bakhtari et al., 1998; Parés et al., 1999; Hirt et al., 2004). A similar magnetic fabric evolution with increasing strain, as seen from field data, is observed in analogue models (Almqvist and Koyi, 2018), with the possibility to differentiate between fabric influenced by thrusting and by grain reorientation due to compaction (Schöfisch et al., 2021).

As a continuation of such modelling studies, in this study, we use the results of a series of shortened sandbox models simulating the evolution of a pop-up structure at different amount of bulk shortening, to investigate the evolution of the magnetic fabric, mainly within an imbricate and at the developed structures. Specifically, the aim of this study is to describe the strain distribution within a pop-up structure and compare the magnetic fabric that develops at different stages of finite strain across the imbricate.

2 Methods

2.1 Model setup and sampling

Three models (A, B, and C) with a similar setup are shortened to different extent in order to analyze the magnetic fabric along thrust faults at different stages that are associated with a development of a pop-up structure (Table 1). To initiate a pop-up structure bounded by active back- and forethrusts, an artificial wedge is sieved and built on top of the model next to the backstop in models A and C. In Model B, a basal plate is attached to the backstop, as a velocity discontinuity, to transmit shortening away from the backstop and initiate a boxfold in the middle of the model away from the backstop. To increase sampling capacity and target individual parts of the boxfold, the models were thick (8 cm) and had an initial dimension of 71x30 cm (Fig. 1). Loose sand was mixed with magnetite grains (<0.1vol%) of the same grain size (0.124-0.356 mm) to enhance magnetic susceptibility. This mixed composition (cohesion = 0.49) was used to construct layers that were scraped to an individual thickness of one centimeter each. Between each 1 cm-thick layer, a thin marker horizon is sieved using different colored sand. To monitor surface deformation, a colored

grid of circles is imprinted on the model surface by sieving. After shortening, the models are carefully wetted, and vertical sections are taken parallel to the shortening direction (Table 1). Each section is photographed, and oriented cubic samples (volume 2.2 cm³) are taken across the sections in specific parts of the structure (forethrust, backthrust, forekink zone, crestal areas, undeformed part in the foreland, etc.) for AMS analyses.

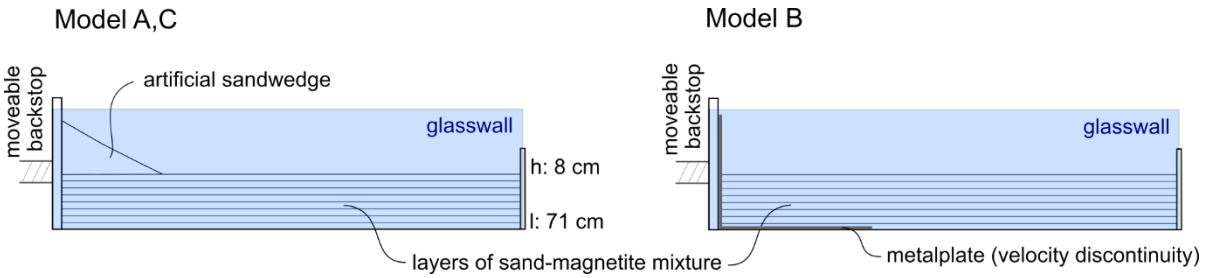

Figure 1: Sketch of model setups. A pre-existing wedge was placed next to the backstop on top of the surface of models A and C. In Model B, a metal plate that moved with the backstop was used as velocity discontinuity.

Table 1: Overview of setup of the three models. The three models share the same thickness and lateral dimensions but vary in the amount of bulk shortening and sampling.

	bulk shortening	setup variation	secti
Model A	12 cm = 16%		8 / 2
Model B	17.5 cm = 24.5%	velocity discontinuity by underlying moving metal plate; length: 20 cm	7 / 3
Model C	24 cm = 34%		5 / 1

2.2 AMS measurements and fabric evolution

AMS measurements were performed with a MFK1-FA Kappabridge (Agico Inc.) using an AC field strength of 200 A/m and a frequency of 976 Hz. From each measurement, the bulk orientation of the principal axes of susceptibility (k_{max} k_{int} k_{min}) of magnetite grains within one sample is calculated and plotted on a lower-hemisphere equal-area projection with the backstop defining the North. Note that the matrix sand, consisting mainly of weakly diamagnetic quartz, is considered to have a negligible contribution to the AMS compared to the magnetite. Furthermore, the principal axes define an ellipsoid, which can be described by the shape of anisotropy ($T = [2n_{int} - n_{max} - n_{min}]/[n_{max} - n_{min}]$) and degree of anisotropy ($Pj = exp\{2(n_{max} - n_{mean})^2 + (n_{int} - n_{mean})^2 + (n_{min} - n_{mean})^2]\}$) with $n_{max} = ln(k_{max})$, $n_{int} = ln(k_{int})$, $n_{min} = ln(k_{min})$, and $n_{mean} = (n_{max} + n_{int} + n_{min})/3$ (Jelinek, 1981; Hrouda, 1982). The shape of anisotropy (T) ranges from T = -1 for prolate, $T = 0$ for neutral to $T = +1$ for oblate ellipsoids. The degree of anisotropy describes a ratio between the principal axes, hence a change in the alignment of the magnetic grains

(magnetite in this model) within a sample will result in a different degree of anisotropy (Hrouda, 1982), e.g., high values indicate a preferred orientation. Analyzing the magnetic fabric throughout the model enables a description of strain changes due to principal axes rotation and it is used to describe a strain path from an oblate depositional fabric towards an intermediate and tectonic fabric with lower *Pj* and occurrence of more prolate susceptibility ellipsoids (e.g., Kligfield et al.,1981; Rochette et al., 1992; Borradaile and Henry, 1997; Bakhtari et al., 1998). Note that since we neither model ductile deformation, grain fracturing nor recrystallisation, which influence the bulk orientation of the magnetic fabric in cleavages zones (Borradaile and Tarling, 1981; Hirt et al., 2004; Ferré et al., 2014), the magnetic fabric development is limited to rigid body rotation of grains in our models. However, a reworking of the magnetic fabric due to rigid body rotation caused by an increase in LPS, folding and thrusting are often interpreted for FTBs (e.g., Averbuch et al., 1992; Borradaile and Henry, 1997; Bakhtari et al., 1998; Saint-Bezar et al., 2002; Burmeister et al., 2009) and are observed in analogue models (Almqvist and Koyi, 2018; Schöfisch et al., 2021).

3 Results

3.1 Model kinematics and evolution

The three models (Models A, B and C) are shortened to different amounts (12 cm, 17.5 cm, and 24 cm, respectively) (Table 1), but share a relatively similar evolution and comparable development of structures. The main structure that developed during the shortening of the models is a pop-up structure with a well-defined backthrust and a broad forekink zone (Figs. 2a, b, and c). In addition to the pop-up structure, the models developed other structures in their foreland. For example, in front of the pop-up structure in Model A (16% bulk shortening), two new forekinks were initiated as indicated by bending of the surface markers and slight increase in topography (dashed lines in Fig. 2b). These forekinks represent an early stage of forethrust creation. In Model B (24.5% bulk shortening), an additional forethrust (FT1) developed simultaneously with the splay of the backthrust (BT) of the major pop-up structure. Farther into the foreland of Model B, a second forethrust (FT2) formed, represented by a mm-scale fore-kink (Fig. 2b). However, compared to models A and B, Model C (34% bulk shortening) developed a more complex set of structures (Fig. 2c). In this model, a "lower" backthrust (BT1) formed simultaneously with the "upper" forekink zone (FKZ1). At a later stage, an "upper" gently-dipping backthrust (BT2) formed and uplifted FKZ1. Simultaneously with initiation of BT2, a "lower" forekink zone formed (FKZ2). With further shortening, a second pop-up structure formed in the foreland. This additional foreland-pop-up consists of a narrower forekink zone (FKZ3) and a foreland-backthrust (BT3). This BT3 offsets the upper layers of the FKZ2, which in turn is offset by a forethrust (FT) that initiated during further shortening (after 21 cm of shortening, representing 90% of final bulk shortening of Model C). This FT, located beneath FKZ2, splayed and is related to the deformation of the main pop-up structure, where a

new backthrust is about to form above BT2 as counterpart (Fig. 2c, dashed red line in Model C above BT 2) (Fig. 2c). Overall, the three models show a similar evolution of a pop-up structure at different stages of shortening (Figs. 2a, b, and c). Faults and kinks in each model steepen with depth and displacement along all faults decreases with depth (Figs. 2d, e, and f).

3.2 Cross-section balancing

During shortening of the models, strain is partitioned between the three deformation components: layer-parallel shortening (LPS), folding, and thrusting. The amount of deformation taken up by thrusting and folding is proportional to the percentage of bulk shortening. However, most of the strain in all models is accommodated by LPS, i.e., penetrative strain (Figs. 2d, e, and f). Even though LPS increases with bulk shortening, its contribution to the overall strain decreases relative to that of folding and thrusting with progressive bulk shortening. In general, the amount of LPS and folding are changing with depth in all models, whereas thrusting decreases (Figs. 2d, e, and f). Additionally, the distribution of strain and its trend with depth is different in Model B compared to models A and C (Figs. 2d, e, and f). In Model B, LPS decreases from the surface to layer 4 and then increases again towards the deeper layers (Fig. 2e), whereas the opposite is the case for folding. Thrusting in Model B mainly decreases with depth as seen in models A and C (Figs. 2d, e, and f).

3.3 Magnetic fabric

In the three models, 779 samples were taken and analyzed for AMS signature (Table 1). We separated the datasets from the models by their location relative to the main structures (thrusts and forekink zone) and describe the characteristic magnetic fabric in detail in the following sections. The distance of a sample to a thrust or a kinkzone is measured by using the center of the sample. Consequently, we assume that samples, whose centers are lying in a range of 0.8 cm (length from center to corner of the cubic samples) to a thrust or kinkzone, are carrying a signal that is attributed to thrust or kinkzone and are summarized within the datasets showing magnetic fabrics of such a structure. The complete dataset is provided in the data repository (Schöfisch, 2021) and an overview of AMS distribution across the pop-up structures are presented as supplementary material (S1-S8).

3.3.1 M*agnetic fabric away from thrust and kinkzone*

An oblate shape of anisotropy, where kmin axes are clustered vertically relative to bedding, is observed in all models in areas away from a thrust or kinkzone, i.e., the footwall of the backthrusts next to the backstop, the interlimb zone between the main backthrust and main forekink zone, and the areas between the "minor foreland" thrusts in front of the main forekink zones (Fig. 3). Both kmax and kint define a horizontal to subhorizontal magnetic foliation around the primitive circle parallel to the sand layers in these areas, where kmax is generally aligned along the model north (towards backstop)-south axis, and kint clusters mainly in the east and

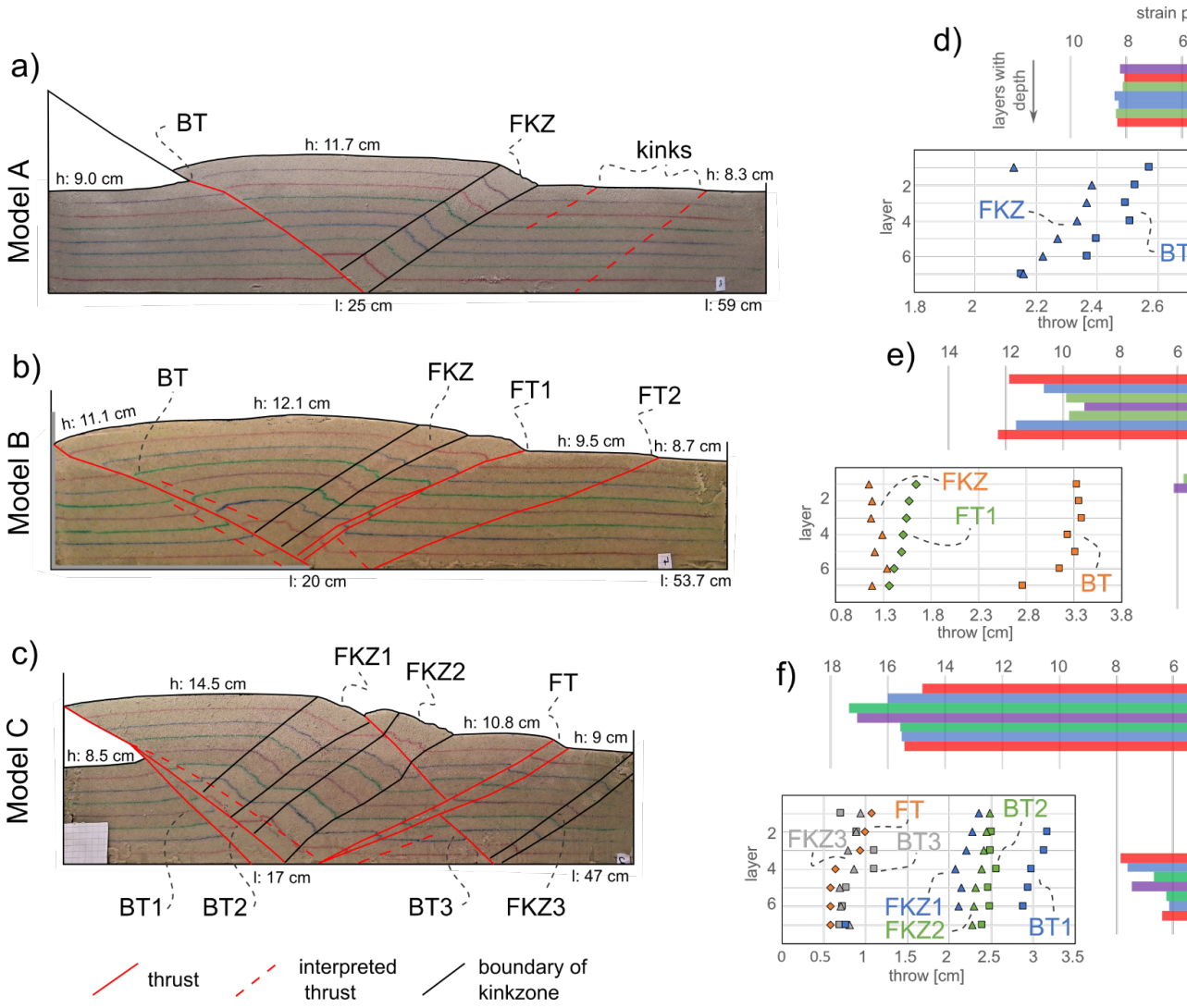

Figure 2: Three models A,B,C are shortened to different amount of bulk shortening (16%, 24.5%, 34%). They show the evolution of a pop-up structure. a,b,c) show representative cross-sections for each model. d,e,f) show the restoration of cross-sections, which provide a partitioning of strain. Additionally, the heave at major structures is plotted for each layer counting from the top.

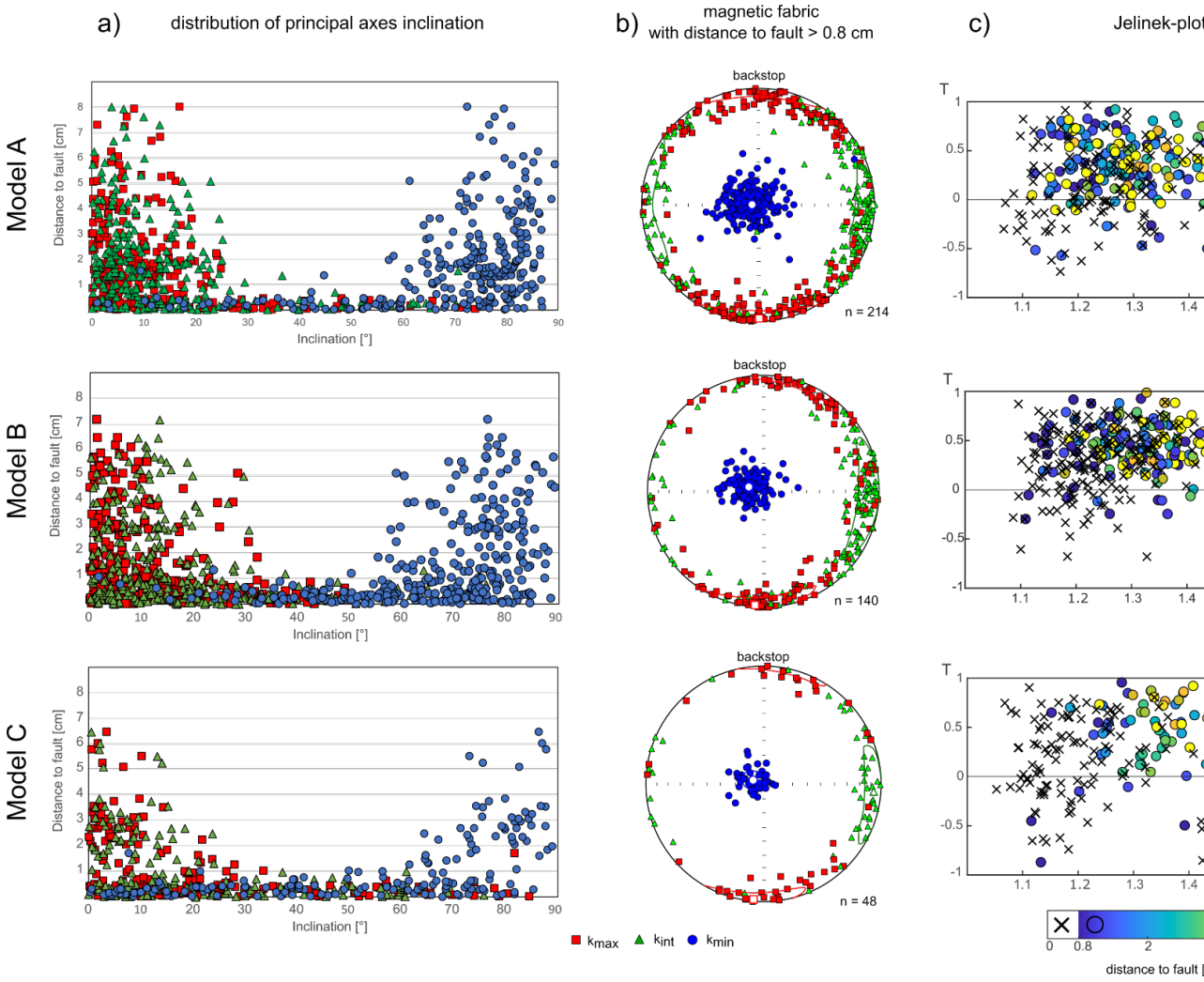

Figure 3: a) plots of the inclination of the principal axes (kmax kint kmin) as a function of distance to a thrust or kinkzone. b) equal-area projection showing distribution of principal axis for samples with a distance > 0.8 cm to a thrust or kinkzone with backstop to the North. c) illustrates the distribution of degree and shape of anisotropy using the Jelinek-plot. Circles coincide with samples taken away from a thrust of kinkzone, whereas crosses represent data from thrust and kinkzone.

west direction (Fig. 3b). The degree of anisotropy in these areas lies in the interval between 1.1 Pj 1.6 (Fig. 3c).

All three models show a general trend in principal axes rotation as a function of distance to a thrust or kinkzone (Fig. 3a). The closer the sample is to such

a structure, the larger is the variety of inclinations of the principal axes, e.g., kmax and kint axes rotate from mainly horizontal inclinations to broad range of inclinations (Fig. 3a). The opposite is observed for the inclination of kmin axes. The degree of anisotropy (Pj) generally decreases towards a thrust or kinkzone (Fig. 3c). Furthermore, the shape of anisotropy is oblate for most of the samples away from a thrust or kinkzone, whereas in the vicinity of a such structure both prolate and oblate shapes are observed (Fig. 3c).

3.3.2 *Magnetic fabric at thrust surfaces*

An evolution of magnetic fabric for thrusts can be recognized in the models. The thrusts from the models show different amounts of displacement and therefore the observed magnetic fabric at each thrust can be related to the different degree of thrust maturity (Figs. 2, and 4).
The kinks in front of the pop-up structure in Model A are described as an early stage of thrust development and samples from the kinks show vertical k_{min} axis distribution with horizontal k_{max} and k_{int} axes. The principal axes orientation of the kinks is similar to the principal axes orientation observed in samples away from the thrusts or kinkzones (Fig. 4a). Nevertheless, samples from the kinks show a lower degree of anisotropy (Pj) with some tendency towards a prolate fabric, which is different compared to samples away from thrusts and kinkzones (Figs. 3c, 5a, and 5d).
The principal axes for samples from the forethrust (FT2) in the foreland of Model B are less clustered, as observed for the kinks in Model A (Fig. 4a). Additionally, at FT2, k_{max} and k_{int} create a magnetic foliation that is subhorizontal (dipping 10-20°) and are therefore not as horizontal as observed for samples away from the thrusts, but also not parallel to the thrust surface. k_{min} axes clusters tightly around the mean, with a steep inclination (~80°) that verges slightly to the south-west (Fig. 4a). The degree of anisotropy for samples taken at FT2 is generally lower than for data collected at the kinks in the foreland of Model A. However, the peaks of the distribution of the degree of anisotropy for data from FT2 and the kinks in Model A are similar (Fig. 5d).
The forethrust (FT) of Model C as well as the splayed forethrust (FT1) of Model B developed a magnetic foliation that converges into the orientation of the thrusts (Fig. 4a). For both forethrusts, most of the principal axes developed a subhorizontal magnetic foliation (i.e., girdle distribution of k_{max} and k_{int}) that tends into parallelism with the forethrusts and k_{min} axes started to rotate from vertical towards gentler inclinations in the south (Fig. 4a). Additionally, the degree of anisotropy at both forethrusts (FT and FT1) is comparable and is lower than observed for the kinks in Model A and FT2 in Model B (Fig. 5).

Along the backthrusts of all three models, k_{max} and k_{int} develop a magnetic foliation parallel to the thrust surfaces with k_{min} clustering at the pole (Fig. 4b). However, some principal axes deviate from this general alignment and clustering, which can be attributed to the local structural complexity and splaying of the backthrusts. Along the backthrust of Model B, a clustering of k_{max} indicate a clustering of magnetic lineation (k_{max}) parallel to the north-south shortening

direction (Fig. 4b). In all thrusts (fore- and backthrusts) of the three models, a decrease in the degree of anisotropy can be observed downwards along the thrust surfaces, i.e., Pj decreases with depth for each thrust (Fig. 4d). Despite that the thrusts show different amount of displacement (Fig. 2), degree of anisotropy is still comparable between all thrusts (1.1 Pj 1.4), except for the kinks (early-stage thrusts) in the foreland of Model A, which have slightly higher degree of anisotropy (1.15 Pj 1.5) (Fig. 5). At depth, where thrusts are intersecting, slightly higher degree of anisotropy are observed. For example, at 8 – 13 cm depth interval of the backthrust in Model C, the forekink zones are intersecting with the backthrust and a slightly higher degree of anisotropy is calculated (Fig. 5). The shape of anisotropy at the thrusts is classified as a mix between prolate and oblate shapes (Fig. 3c). Nevertheless, the oblate shapes dominate at the thrusts (Fig. 3c).

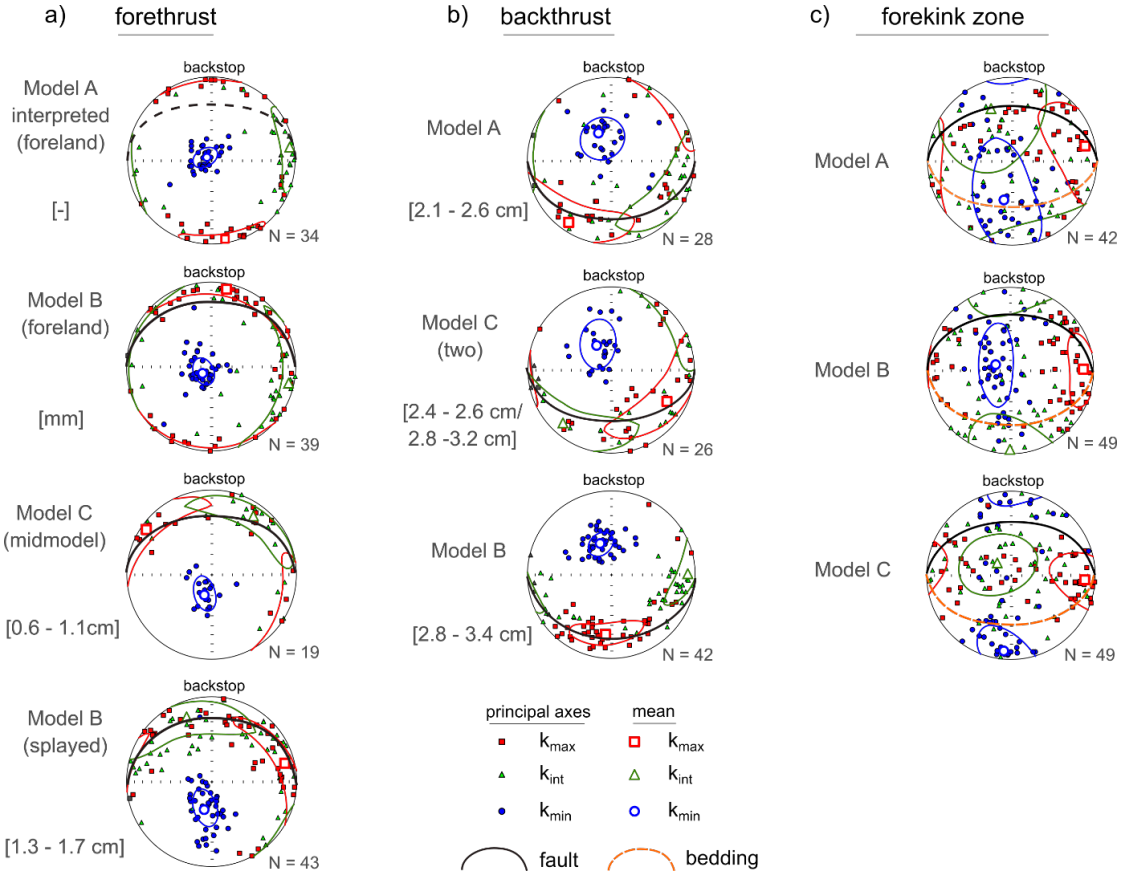

Figure 4: Equal-area projections showing principal axes of magnetic susceptibility with their means and 95 % confidence ellipses of the means (ellipses with same color as principal axes) from a) the forethrusts, b) backthrusts, and from c) the forekink zones from the three models A, B, and C with backstop to the

North. The numbers in the brackets are the ranges in displacement along each thrust.

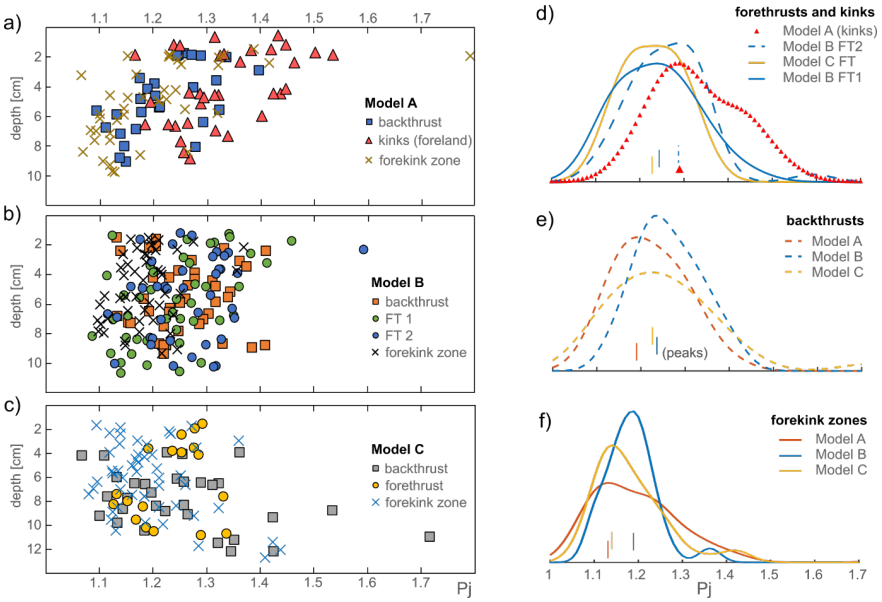

Figure 5: Distribution of degree of anisotropy (Pj) with depth for a) Model A, b) Model B, and c) Model C. The density of distribution probabilities, calculated with a Kernel distribution function, of the degree of anisotropy for each structure from the models are given in d) for forethrusts and foreland kinks, e) backthrusts, and f) forekink zones. The position of the peak values (maxima) of each curve in d,e, and f are plotted with short vertical lines in the same color along the x-axis.

3.3.3 *Magnetic fabric in forekink zone*

The magnetic fabric within the relatively broad forekink zones can be summarized by principal axes spreading along north-south and east-west oriented great circle girdles (Fig. 4c). The forekink zone in Model A developed a scattered broad k_{max}-k_{int} girdle (i.e., magnetic foliation) dipping to the north with a sub-horizontal mean of k_{max} towards east and a mean of k_{int} that is dipping ~35° to the north. In contrast, k_{min} scatters as a broad north-south girdle with inclinations that vary from vertical to horizontal. Nevertheless, the mean of k_{min} is directed towards the south with an inclination of 52°, although with a very large mean confidence ellipse (Fig. 4c). By comparison, in the forekink zone of Model B, k_{min} developed a broad north-south girdle distribution as well, but with a narrower confidence ellipse and a mean clustering of k_{min} that is almost vertical (Fig. 4c). Furthermore, in the forekink zone of Model B, k_{max} is mainly clustering along an east and west axis, defining a magnetic lineation perpendicular to the shortening direction. The k_{int} axes of the forekink zone in Model B rotated into the north-south girdle distribution of k_{min} with a horizontal k_{int} mean axis

aligned north-south. The two forekink zones in Model C developed a general principal axes distribution that can be compared to the magnetic fabric in the forekink zone of Model A (Fig. 4c). In the two forekink zones of Model C, k_{max} and k_{int} define a magnetic foliation trending perpendicular to the shortening direction with different inclinations but mainly with a vertical k_{int} mean and a suhorizontal east-west k_{max} mean. The k_{min} axes cluster subhorizontally in the two forekink zones of Model C with a north-south direction with a mean k_{min} plunging subhorizontally towards the south in the lower hemisphere projection (Fig. 4c). Notably, the minor forekink zone in the foreland of Model C (FKZ3) developed a similar AMS pattern as seen in the major forekink zones in this model (i.e., FKZ1 and 2). Overall, the shape anisotropy observed in forekink zones from all the three models are heterogeneous and range from oblate to prolate. The degree of anisotropy is comparable between the forekink zones of all three models and range from 1.05 Pj 1.35, which are the lowest ranges observed in this study (Fig. 5f). However, the peak of the distribution of the degree of anisotropy of the kinkzone in Model B is higher than the peaks for the forekink zones of Model A and Model C. (Fig. 5f).

4 Discussion

4.1 Strain distribution across the models

Of the three components of shortening (LPS, folding, and thrusting), LPS is dominant at the early stage of model deformation, leading to compaction of the shortened layers until folds and thrusts accommodate the shortening resulting in formation of an imbricate (Mulugeta and Koyi, 1992, Koyi, 1995, Koyi et al., 2003). This is also illustrated by our models, where the amount of LPS increases with bulk shortening but with a gradual decrease in strain accommodation giving way to an increase in faulting and folding as the imbricate is uplifted along the backthrust(s). Displacement of layers by faulting and folding are visible components of deformation during model shortening and localizes at certain zones within the models. Nevertheless, LPS, which is accommodated by grain rotation and repacking (Fig. 2), is not easy to identify by naked eye. Processes like compaction, grain rearrangement and grain reorientation contribute to the overall LPS and are consequences of stress propagation through the model (Koyi et al., 2003). However, since AMS monitors grain orientation and alignment, it can be used to indirectly deduce the degree of compaction and hence penetrative strain distribution. Reworking of the magnetic fabric due to an increase in LPS, folding and thrusting is typical for FTBs (e.g., Averbuch et al., 1992; Borradaile and Henry, 1997; Bakhtari et al., 1998; Saint-Bezar et al., 2002; Burmeister et al., 2009) and is a process that is observed in the three models presented in this study. All three models are shortened to different amount of bulk shortening, but express similar distribution of principal axes of magnetic susceptibility, degree of anisotropy (Pj) and shape of anisotropy (T). In general, there is a distinct difference between a magnetic fabric that developed away from a thrust or kinkzone to that within a thrust or kinkzone (Figs. 3 and 4). Consequently, the AMS data show (i) a change in the magnetic fabric as a function of distance

to a thrust or kinkzone (Figs. 3a and 3c), and (ii) clear tectonic overprinting of a pre-existing magnetic fabric at faults and kinkzones.

4.1.1 *Compaction and folding in areas away from thrust and kinkzone*

Areas away from thrusts and kinkzones show a magnetic fabric that can be classified as a mixture between the initial fabric and tectonic fabric, where the tectonic fabric is represented by mainly LPS. The initial fabric is determined by model preparation as scraping produced an alignment of a magnetic lineation parallel to the shortening direction with k_{min} vertical to bedding (Almqvist and Koyi, 2018; Schöfisch et al., 2021). This initial fabric is preserved in some places, regardless of distance to a thrust or kinkzone (Fig. 3b). However, a variation in principal axes distribution is illustrated by the distribution of k_{max} and k_{int} axes around the primitive circle with horizontal to subhorizontal (~10-20° dipping) inclinations (Fig. 3b). The change in magnetic fabric in the areas away from thrusts and kinkzones can be attributed to mainly penetrative strain, i.e., LPS (Fig. 2a). This agrees with observations of the penetrative-strain induced fabric from other modelling studies (Almqvist and Koyi, 2018; Schöfisch et al. (2021) and natural examples (Kissel et al., 1986; Lee et al., 1990; Averbuch et al., 1992; Bakhtari et al., 1998; Parés and van der Plujim, 2002; Sans et al., 2003) where k_{max} is aligned perpendicular to the shortening direction and k_{min} remained vertical (pole to bedding). However, also gentle folding can be interpreted in the areas away from thrusts and kinkzones as bedding changes slightly along profile (Fig. 2). Folding is responsible for the change in inclination of the magnetic foliation, as k_{max} and k_{int} remain parallel to bedding, which has been reported by Averbuch et al. (1992) and Saint-Bezar et al. (2002). Consequently, the grain reorientation in areas away from thrusts and kinkzones, as described by the magnetic fabric, is characterized by tectonic compaction and folding. However, folding, i.e., bedding rotation in the areas away from thrusts and kinkzones, is very gentle and responsible for only few degrees, up to maximum 10°, of inclination change of magnetic foliation.

Despite the variation in orientation of the principal axis, the degree of anisotropy for samples away from thrust and kinkzone illustrate a broad range of values (1.1 Pj 1.6). In the vicinity of a thrust or kinkzone prolate shape of anisotropy is recognizable, even though the overall fabric is oblate (Fig. 3c). This heterogeneous distribution in orientations of principal axes, degree of anisotropy and shape of ellipsoids (Fig. 3) describe a varying strain in the areas away from thrusts and kinkzones. This is known from observing deformation within an imbricate before fault initiation with optical methods (Adam et al., 2005; Dotare et al., 2016). Adam et al. (2005) described the strain distribution within an imbricate as "diffuse shear strain", whereas Dotare et al. (2016) recognized this "diffuse strain" as an accumulation of several short-lived weak shear bands during compaction of an imbricate. Our model results reveal a further detailed insight into the strain distribution in imbricates, especially, as the AMS data from the models show gradients in change of the magnetic fabric towards a thrust and a kinkzone.

4.1.2 S*train gradient towards thrusts and kinkzones*

Even though the principal axis distribution, degree of anisotropy and shape of anisotropy are scattered and described as a kind of "diffuse strain" in areas away from thrusts and kinkzones, a gradient in these magnetic fabric parameters can be described as a function of the distance to a thrust or kinkzone. With decreasing distance to a thrust or kinkzone, the variation of principal axis inclination increases, and a higher variation of principal axes orientations can be found closer to the thrust or kinkzone (Fig. 3a). Furthermore, a trend of decreasing degree of anisotropy is observed towards a thrust or kinkzone and the presence of prolate fabric increases in areas closer to a fault (Fig. 3c). Similar observations in changes of the magnetic fabric towards a thrust are identified from, for example, the French Alps (Kligfield et al., 1981), Corbières in the Pyrenees (Averbuch et al. 1992), Central Appalachian FTB (Hirt et al., 2004), Gavarnie thrust in the Pyrenees (Marcén et al., 2018), the Barbados Accretionary Prism (Housen et al., 1996), and the Hikurangi Subduction Margin in New Zealand (Greve et al., 2020). Note that the first four studies above show an effect of magnetic mineral reprecipitation, and the latter two studies show an additional effect of fluids on the magnetic fabric. However, observations are similar to what our models show, and there is a compatible decreasing trend in the degree of anisotropy and alignment of magnetic grains towards the faults. Irrespective of the influence of fluids and mineral recrystallisation, our models suggest that brittle deformation plays a major role in reorientation of grains, and changes in magnetic fabric due to tectonic compaction and folding are important mechanisms towards a thrust.

Bulk shortening and hence the amount of deformation in a model, are reflected in the trends and gradients of the magnetic fabric change towards a thrust or kinkzone. With larger bulk shortening, more faults and kinkzones formed in the models, and displacement increased along the structures bounding the main boxfold, i.e., backthrusts and forekink zones. It appears, that with increasing shortening within a model, changes in magnetic fabric between a thrust-induced fabric and magnetic fabric away from thrusts and kinkzones are more distinct. The increase in variety of inclination of the principal axes with decreasing distance to a thrust or kinkzone occurs over smaller distances (Fig. 3a). For example, the largest amount of strain is accommodated in Model C (Fig. 2f), and the change in principal axes inclination as a function of distance to thrust and kinkzone is observed for a smaller distance in this model compared to models A and B, where the gradient is steeper, more linear and is observed over a longer distance (Fig. 3a). Also, the degree of anisotropy shows less scattering and a clearer decrease in Model C (Fig. 3c), which is not a consequence of the differing number of samples between the models (Table 1). Consequently, the transition of a magnetic fabric away from a thrust or kinkzone towards a magnetic fabric at a thrust or kinkzone is defined by the amount of bulk shortening, which is also reflected in the amount of displacement along a thrust.

Furthermore, most studies interpret an increase in strain, especially LPS, from

the foreland to the hinterland in FTBs over a larger regional scale. However, such increase in strain as a function of distance to the hinterland is not linear and it has been observed that accumulation of strain is rather expressed by localized minor faults and deformation zones that accretion towards the hinterland (e.g., Groshong et. al. 1984, Averbuch et al., 1992; Dittmar et al., 1994). However, our models show that strain is also changing and increasing within imbricates, towards its boundaries on a local scale. Consequently, AMS provides useful insights into the strain distribution of an imbricate and therefore the model results encourage studying strain distribution of natural analogues within FTBs at local scales.

4.1.3 *Tectonic overprinting by thrusting*

The magnetic fabric observed at a thrust is distinct from the other sets of magnetic fabric observed in the other areas of the models. Moreover, greatest change in magnetic fabric from the initial fabric is observed at a thrust, especially where the displacements by thrusts are large. Thrusts from all three models, i.e., backthrusts and forethrusts, created a similar fabric pattern that reflects the geometry of the thrusts, as the magnetic foliation (k_{max}-k_{int} girdle) is scattered, generally along a great circle parallel to the thrust plane, instead of being parallel to the bedding (Figs. 4a and b). Consequently, thrusting has a significant impact on the development of the magnetic fabric and such fabric can be described as "thrust-induced fabric" (Schöfisch et al. 2021). Samples from a thrust show a higher variation in the shape of anisotropy with both oblate and prolate shape anisotropy. Compared to LPS-produced fabric in areas away from the thrust, more prolate shapes can be observed with a general lower degree of anisotropy in thrusts (Fig. 3c). The change from oblate to a more prolate fabric with a lower degree in anisotropy is consistently observed in the vicinity of a thrusts in the models and is common in nature as deformation increases and localizes towards a structure (Kligfield et al., 1981; Hirt et al., 2004). In general, changes in magnetic fabric, with magnetic foliation parallel to thrust surface and low degrees of anisotropy, are in agreement with experiments (Borradaile and Alford, 1988; Borradaile and Puumala,1989; Housen et al., 1993; Schöfisch et al., 2021), numerical models (Housen et al., 1993), and field observations (e.g., Averbuch, et al. 1992; Housen et al., 1996; Parés and van der Pluijm, 2002; 2004; Hirt et al., 2004; Marcén et al., 2018; Greve et al., 2020).

AMS analysis show that prominent changes in the degree of anisotropy and alignment of principal axes can be observed at the onset of thrusting (Figs. 4 and 5). The kinks at the front of the main boxfold in Model A and the forethrust in Model B with a minor offset show a mixture between the magnetic fabric observed farther away from the thrust and at more mature thrusts, with larger displacement like the backthrusts (Figs. 3 and 4). Compaction precedes thrusting (e.g., Adam et al., 2005; Dotare et al., 2016) and further kinking takes place before the sand layers are offset by thrusting. Therefore, thrusting will overprint a LPS-affected fabric, that has also a signature of folding. The

kinks in Model A and the forethrust in Model B illustrate a transition from a "compactional fabric" to a "thrust-induced fabric", which occurs with kink initiation and minimal layer offset in our models. This means that compaction, kinking and folding are the main components responsible for principal axes reorientation prior to thrusting.

With larger displacement along a thrust, a "thrust-induced fabric" shows a general alignment of magnetic foliation with the thrust surface. This thrust-induced fabric is seen in the well-developed fore- and backthrusts of all three models (Figs. 3a and b). Especially at the backthrusts, overprinting of a compacted and folded magnetic fabric is more efficient, as deformation within the zone of thrust initiation created alignment of principal axes with the thrust surface (Fig. 3b). Nevertheless, variations in principal axis orientation can occur due to structural complexity, for example, where a fore- and backthrust are intersecting (Model C), or where a splay developed (Model B). Note that an increase of degree of anisotropy at lower levels in the models is related to the intersection of other thrusts (Fig. 5). For example, the backthrust of Model C is intersecting with the forekink zones at depth in the model and an influence on the magnetic fabric is expected in this area (Fig. 6).

As strain, especially LPS, is heterogenous throughout a model (Mulugeta and Koyi, 1992; Koyi, 1995), notably with depth (Koyi et al., 2003), the variation in strain will also be reflected in the magnetic fabric prior to thrusting and can be inherited in further overprinting (e.g., Parés and von der Pluijm, 2002; Ferré et al., 2014; Marcén et al., 2018). The models reported here also show a change in strain with depth (Figs. 2d, e, and f), especially by decreasing displacement along the thrusts (Fig. 2). The changes in displacement and strain accommodation with depth in the models can explain a general decreasing trend in the degree of anisotropy downwards the thrusts (Fig. 5). Relatively higher values in degree of anisotropy reveal a preferred alignment of the magnetic grains within the samples, whereas lower degrees show less preferred alignment of grains (e.g., Borradaile and Jackson, 2010; Parés, 2015). This means that thrusting was less efficient in realigning the grains at depth, and an AMS signal prior to thrusting is inherited in the final modelled magnetic fabric. A similar observation is made at the Gavarnie thrust in the Pyrenees (Marcén et al., 2018), where an intersection lineation prior the Alpine deformation is inherited during reactivation of the thrust and a low degree of anisotropy is observed at the reworked Variscan fabric.

Additionally, the trend of decreasing degree of anisotropy with depth along a thrust seems to be independent of the amount of displacement at a thrust, as the same trend can be interpreted at each thrust from the three models, whereas each thrust differs in amount of displacement. The changes in AMS signal at a thrust needs to be discussed considering relative changes in deformation along an individual thrust instead of comparing absolute numbers of displacement for each thrust. Larger displacement, which is observed in upper segments of the thrusts, produce higher degree of anisotropy and therefore grains are more

aligned compared to deeper segments of the thrusts, where lower displacements and lower degree of anisotropy are observed. However, comparing data between different segments of different thrusts, but with similar amount displacement, is deceiving, because different segments of thrusts and, in general, thrusts from different models have different deformation histories in general.

The trend of decreasing degree of anisotropy with depth at a thrust is less obvious for thrusts in Model B and C compared to thrusts in Model A (Figs. 5a, b, and c). This further emphasizes that strong changes in magnetic fabric are observed at the beginning of thrust initiation, as the thrusts in Model A are less mature compared to the thrusts from the other models. With increasing deformation and further displacement at a thrust, differences in magnetic fabric (e.g., inclination of principal axes or degree of anisotropy) between upper and lower parts of a thrust will decrease. Our models are limited to grain reorientation only and therefore, alignment of principal axes of susceptibility parallel to a thrust will reach a certain degree of anisotropy. However, AMS data from the modelled thrusts reveal "heterogeneous strain" along thrusts and shear zones, which are typical observations in nature (e.g., Ferré et al., 2014). Consequently, this highlights the importance of brittle reorientation of grains during thrust development.

4.1.4 *The internal deformation of kinkzones*

The initial model setup and the amount of bulk shortening are reflected in the evolution of the model and, especially, in the creation of the forekink zones. The geometric variation in width and extent of the forekink zones from the different models, are also expressed in the magnetic fabric for each forekink zone. The forekink zones consist of rotated bedding parallel to the backthrust and many forethrusts with small displacement (Fig. 2). The small displacement (millimeters) within the kinkzone is significant enough to rotate grains, which results in a broad spread of the principal axes of susceptibility (Fig. 4c). Overall, the magnetic fabric in the forekink zones can be described by an interplay among LPS, thrusting, and folding, while folding includes bedding rotation parallel to the backthrust on a larger scale and internal kinking due to forethrust creation on a smaller scale. The different mechanisms of deformation contributed differently in each kinkzone and can be revealed by the magnetic fabric.
The kinkzone fabric from all three models, especially the means of the principal axes of susceptibility and their confidence ellipses, are comparable and summarized by a mean of k_{max} oriented to the East-West and by means of k_{min} and k_{int} within a broad north-south girdle (Fig. 4c). The k_{max} clustering defines a magnetic lineation normal to the shortening direction and parallel to the fold axis of the minor kinks and bedding-thrust intersection within all models. However, the principal axes are rather scattered, which is also reflected by the appearance of low degree of anisotropy, which is even lower than observed at thrusts or in areas away from thrust and kinkzone (Fig. 5). Low degree of anisotropy derives from the intersection of folding and thrusting, without a dominance of either of these deformation processes. This agrees with natural examples, where S-C-

structures are producing a low degree of anisotropy (Ferré et al., 2014; Marcén et al., 2018). However, the composite magnetic fabric needs to be analyzed carefully, because summarizing different grain orientations in a bulk susceptibility makes AMS to strain correlation more difficult (Housen et al., 1993; Ferré et al., 2014). In contrast, at the intersection between backthrust and forekink zone, e.g., in Model C, the intersection is well defined and produces a relatively higher degree of anisotropy compared to the interplay of thrusting and folding in the kinkzones itself.

As bedding within the forekink zone is generally parallel to the backthrust, the magnetic fabric depicts this bedding rotation. Several previous studies have shown that the magnetic foliation remains parallel to the bedding during folding (Averbuch et al., 1992; Bakhtari et al., 1998; Saint-Bezar et al., 2002). However, the models presented in this study show that several minor forethrusts are developed within a forekink zone. Consequently, the fabric in these forekink zones is not only the product of bedding rotation, but the effect of thrusting needs to be considered too. In a steep forekink zone inclination, which cause larger throw, thrusting within the kinkzone will have a greater impact on AMS signature, as seen in Model A by the development of broad gridle of k_{max} and k_{int} subparallel to the fault surface (Figs. 2 and 4c). An even clearer magnetic foliation and clustering of k_{min} (seen by narrower confidence ellipses compared to forekink zone in Model A) is observed in the forekink zones of Model C (Fig. 4c). However, in the kinkzones of Model C, the magnetic foliation does not align with the forethrust and is rather parallel to the intersection lineation of bedding and forethrusts of the forekink zone. Nevertheless, k_{min} distribution of the kinkzones in Model A and C are clustering to the pole of the forethrusts within the kinkzones. AMS data from the forekink zone in Model B create compatible narrow confidence ellipses as the forekink zones in Model C, but here the position of k_{min} and k_{int} are swapped (Fig. 4c). Obvious step-like kinks developed in the forekink zone in Model B (Fig. 2b), which are less visible in the other models. Consequently, additional internal folding needs to be discussed for the forekink zone of Model B, which explains, that k_{min} is rather distributed in a girdle as poles to the internal folds instead of clustering perpendicular to the thrust surface. However, k_{max} lineation is still parallel to the intersection of the forethrusts and bedding in the forekink zone of Model B, as observed in all forekink zones of all models. Generally, the magnetic fabric highlights the influence of different deformation processes within a kinkzone and reveals strain in more detail.

The observation that the "kinkzone fabric" in the models is a consequence of an interplay between folding and faulting is similar to the observation of Greve et al. (2020). In Greve et al. (2020), the zone right above the major fault zone, called the 'mid hangingwall' in their study, is pervaded by thrusts and has steep bedding. The analyzed AMS fabric from this zone is very similar to the "kinkzone fabric" in our models, where k_{max} clusters perpendicular and a k_{int}-k_{min} girdle is defined parallel to the shortening direction. Another comparison can be done with observations from the shear zone at the Gavarnie thrust

in the Pyrenees (Marcén et al., 2018). S-C-structures create a composite magnetic fabric producing magnetic lineation parallel to the intersection of S- and C-planes. Similar magnetic lineation is produced in our case by the intersection of folding and thrusting. In general, it is known from natural examples, that the intersection of bedding and cleavage in a deformed rock creates a magnetic lineation parallel to it (e.g., Borradaile and Tarling, 1981; Kligfield et al., 1981; Parés and van der Pluijm, 2002; Hirt et al., 2004). However, competing fabric within in one AMS sample lead to a composite fabric, that may not reflect the strain within the deformation zone (Housen, 1993; Ferré et al., 2014). Nevertheless, AMS data from the modelled kinkzones can be associated to different accommodation of deformation within the kink zone as described above. Consequently, AMS reveals different contributions to strain within the kinkzone and vice versa, different deformation processes within a kinkzone lead to complex sets of heterogenous kinkzone fabric.

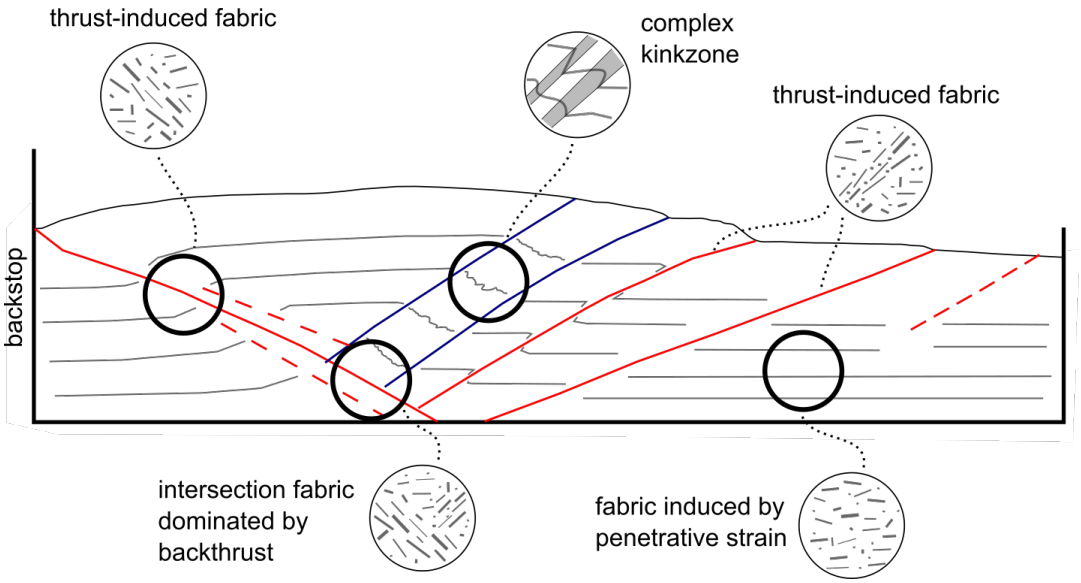

Figure 6: Schematic sketch of grain alignment in the models.

5 Conclusions

Measurements of the magnetic fabric in three different shortened analogue models describe strain distribution across a thrust imbricate, i.e., pop-up structure with associated thrusts and kinkzones. The AMS data reflect a strain gradient from (i) an initial to compactional magnetic fabric towards a (ii) thrust-induced fabric or (iii) composite fabric within forekink zones (Fig. 6). Generally, the geometry of a thrust determines the alignment of the magnetic fabric shown by clustering and girdle distribution of the principal axes. In contrast, folded layers displaced by minor thrusts display a more complicated AMS pattern within the kinkzones. However, fabric analysis in the kinkzones indicates the importance

of strain accommodation of different deformation mechanism like thrusting or folding. In addition, at thrusts, AMS signatures from deformation prior thrusting can be inherited in the finite magnetic fabric, which explains a varying strain distribution and interpretation along thrusts in general. Overall, this AMS study outlines strain distribution and magnitude within different parts of an imbricate in more detail. Strain is changing as function of distance towards localized deformation zones (e.g., thrusts and kinkzones) and with larger bulk shortening, the change in strain between areas away and within deformation zones is more distinct.

Acknowledgement
This study is supported by a research grant from the Swedish Research Council to HK and BA (VR 2017-04519). The authors acknowledge LKAB Minerals Luleå (Sweden) for providing the magnetite for modelling. We thank the editor for editorial handling, and anonymous reviewers for constructive comments. There are no conflicts of interest.

Data Availability Statement

AMS data from the three models of this study will be available at doi:10.17632/zs7n4t57k4.1, an open-source online data repository hosted at Mendeley Data (Schöfisch, 2021). Additionally, uncommented plots illustrating magnetic fabric distribution in the models can be found in the supporting information (Figures S1-S8).

References

Adam, J., Urai, J. L., Wieneke, B., Oncken, O., Pfeiffer, K., Kukowski, N., et al. (2005). Shear localisation and strain distribution during tectonic faulting - New insights from granular-flow experiments and high-resolution optical image correlation techniques. Journal of Structural Geology, 27(2), 283–301. https://doi.org/10.1016/j.jsg.2004.08.008Almqvist, B. S. G., & Koyi, H. (2018). Bulk strain in orogenic wedges based on insights from magnetic fabrics in sandbox models. Geology, 46(6), 483–486. https://doi.org/10.1130/G39998.1Averbuch, O., Frizon de Lamotte, D., & Kissel, C. (1992). Magnetic fabric as a structural indicator of the deformation path within a fold-thrust structure: a test case from the Corbières (NE Pyrenees, France). Journal of Structural Geology, 14(4), 461–474. https://doi.org/10.1016/0191-8141(92)90106-7Bakhtari, H. R. ., Frizon de Lamotte, D. ., Aubourg, C. ., & Hassanzadeh, J. . (1998). Magnetic fabrics of Tertiary sandstones from the Arc of Fars (Eastern Zagros, Iran). Tectonophysics, 284, 299–316. https://doi.org/PIIS0040-1951(97)00179-0Borradaile, G. J., & Puumala, M. A. (1989). Synthetic magnetic fabrics in a plasticene medium. Tectonophysics, 164(1), 73–78. https://doi.org/10.1016/0040-1951(89)90235-7Borradaile, G.J., & Henry, B. (1997). Tectonic applications of magnetic susceptibility and its anisotropy. Earth-Science Reviews, 42(1–2), 49–93. https://doi.org/10.1016/S0012-8252(96)00044-XBorradaile, G J, & Alford, C. (1988). Experimental shear zones and magnetic fab-

rics. Journal of Structural Geology, 10(8), 895–904.Borradaile, Graham J., & Jackson, M. (2010). Structural geology, petrofabrics and magnetic fabrics (AMS, AARM, AIRM). Journal of Structural Geology, 32(10), 1519–1551. https://doi.org/10.1016/J.JSG.2009.09.006Borradaile, Graham J., & Tarling, D. H. (1981). The influence of deformation mechanisms on magnetic fabrics in weakly deformed rocks. Tectonophysics, 77(1–2), 151–168. https://doi.org/10.1016/0040-1951(81)90165-7Burmeister, K. C., Harrison, M. J., Marshak, S., Ferré, E. C., Bannister, R. A., & Kodama, K. P. (2009). Comparison of Fry strain ellipse and AMS ellipsoid trends to tectonic fabric trends in very low-strain sandstone of the Appalachian fold-thrust belt. Journal of Structural Geology, 31(9), 1028–1038. https://doi.org/10.1016/j.jsg.2009.03.010Dahlen, F. A., Suppe, J., & Davis, D. (1984). Mechanics of Fold-and-Thrust Belts and Accretionary Wedges: Cohesive Coulomb Theory. Journal of Geophysical Research, 89(B12), 10087–10101. https://doi.org/10.1029/JB089iB12p10087Davis, D., Suppe, J., & Dahlen, F. A. (1983). Mechanics of fold-and- thrust belts and accretionary wedges. Journal of Geophysical Research, 88(B2), 1153–1172. https://doi.org/10.1029/JB088iB02p01153Dittmar, D., Meyer, W., Oncken, O., Schievenbusch, T., Walter, R., & von Winterfeld, C. (1994). Strain partitioning across a fold and thrust belt: the Rhenish Massif, Mid-European Variscides. Journal of Structural Geology, 16(10), 1335–1352. https://doi.org/10.1016/0191-8141(94)90001-9Dotare, T., Yamada, Y., Adam, J., Hori, T., & Sakaguchi, H. (2016). Initiation of a thrust fault revealed by analog experiments. Tectonophysics, 684, 148–156. https://doi.org/10.1016/j.tecto.2015.12.023Ferré, E. C., Gébelin, A., Till, J. L., Sassier, C., & Burmeister, K. C. (2014). Deformation and magnetic fabrics in ductile shear zones: A review. Tectonophysics, 629(C), 179–188. https://doi.org/10.1016/j.tecto.2014.04.008Graham, J. W. (1966). Significance of Magnetic Anisotropy in Appalachian Sedimentary Rocks. In The Earth Beneath the Continents: A Volume of Geophysical Studies in Honor of Merle A. Tuve. (1966), Geophys. Monogr. Ser., vol. 10, edited by J. S. Steinhart and T. J. Smith, pp. 627-648, AGU, Washington, D. C. (pp. 627–648). https://doi.org/10.1029/GM010p0627Graveleau, F., Malavieille, J., & Dominguez, S. (2012). Experimental modelling of orogenic wedges: A review. Tectonophysics, 538–540, 1–66. https://doi.org/10.1016/j.tecto.2012.01.027Greve, A., Kars, M., Zerbst, L., Stipp, M., & Hashimoto, Y. (2020). Strain partitioning across a subduction thrust fault near the deformation front of the Hikurangi subduction margin, New Zealand: A magnetic fabric study on IODP Expedition 375 Site U1518. Earth and Planetary Science Letters, 542, 116322. https://doi.org/10.1016/j.epsl.2020.116322Groshong, R. H., Pfiffner, A., & Pringle, L. R. (1984). Strain partitioning in the Helvetic thrust belt of eastern Switzerland from the leading edge to internal zone. Journal of Structural Geology, 6(1), 5–18.Groshong, Richard H. (2019). Area-constant strain and dilation in sandbox models: Insights from whole-model area balance. Journal of Structural Geology, 118(November 2018), 279–283. https://doi.org/10.1016/j.jsg.2018.11.003Gutscher, M. A., Kukowski, N.,

Malavieille, J., & Lallemand, S. (1996). Cyclical behavior of thrust wedges: Insights from high basal friction sandbox experiments. Geology, 24(2), 135–138. https://doi.org/10.1130/0091-7613(1996)024<0135:CBOTWI>2.3.CO;2Hirt, A. M., Lowrie, W., Lüneburg, C., Lebit, H., & Engelder, T. (2004). Magnetic and mineral fabric development in the ordovician Martinsburg Formation in the Central Appalachian Fold and Thrust Belt, Pennsylvania. Geological Society Special Publication, 238(1995), 109–126. https://doi.org/10.1144/GSL.SP.2004.238.01.09Housen, B. A., Richter, C., & van der Pluijm, B. A. (1993). Composite magnetic anisotropy fabrics: experiments, numerical models and implications for the quantification of rock fabrics. Tectonophysics, 220(1–4), 1–12. https://doi.org/10.1016/0040-1951(93)90219-AHousen, B. A., Tobin, H. J., Labaume, P., Leitch, E. C., Maltman, A. J., Shipley, T., et al. (1996). Strain decoupling across the decollement of the Barbados accretionary prism. Geology, 24(2), 127–130. https://doi.org/10.1130/0091-7613(1996)024<0127:SDATDO>2.3.CO;2Hrouda, F. (1982). Magnetic anisotropy of rocks and its application in geology and geophysics. Geophysical Surveys, 5(1), 37–82. https://doi.org/10.1007/BF01450244Huiqi, L., McClay, K. R., & Powell, D. (1992). Physical models of thrust wedges. In Thrust Tectonics. https://doi.org/10.1007/978-94-011-3066-0_6Jelinek, V. (1981). Characterization of the magnetic fabric of rocks. Tectonophysics, 79(3–4), T63–T67. https://doi.org/10.1016/0040-1951(81)90110-4Kissel, C., Barrier, E., Laj, C., & Lee, T. -Q. (1986). Magnetic fabric in "undeformed" marine clays from compressional zones. Tectonics, 5(5), 769–781. https://doi.org/10.1029/TC005i005p00769Kligfield, R., Owens, W. H., & Lowrie, W. (1981). Magnetic susceptibility anisotropy, strain, and progressive deformation in Permian sediments from the Maritime Alps (France). Earth and Planetary Science Letters, 55(1), 181–189. https://doi.org/10.1016/0012-821X(81)90097-2Koyi, H. (1997). Analogue modelling: From a qualitative to a quantitative technique - A historical outline. Journal of Petroleum Geology, 20(2), 223–238. https://doi.org/10.1111/j.1747-5457.1997.tb00774.xKoyi, H. A., & Maillot, B. (2007). Tectonic thickening of hanging-wall units over a ramp. Journal of Structural Geology, 29(6), 924–932. https://doi.org/10.1016/j.jsg.2007.02.014Koyi, H. A., Sans, M., Teixell, A., & Zeyen, H. (2003). The Significance of Penetrative Strain in the Restoration of Shortened Layers-Insights from Sand Models and the Spanish Pyrenees. Thrust Tectonics and Hydrocarbon Systems: AAPG Memoir., 82, 1–16. Retrieved from http://gent.uab.cat/ateixell/sites/gent.uab.cat.ateixell/files/16.-Koyietal03.pdfKoyi, Hemin. (1995). Mode of internal deformation in sand wedges. Journal of Structural Geology, 17(2), 293–300. https://doi.org/10.1016/0191-8141(94)00050-AMaillot, B., & Koyi, H. (2006). Thrust dip and thrust refraction in fault-bend folds: Analogue models and theoretical predictions. Journal of Structural Geology, 28(1), 36–49. https://doi.org/10.1016/j.jsg.2005.10.001Maillot, B., & Leroy, Y. M. (2003). Optimal dip based on dissipation of back thrusts and hinges in fold-and-thrust belts. Journal of Geophysical Research: Solid Earth, 108(B6), 1–17. https://doi.org/10.1029/2002jb002199Marcén, M., Casas-Sainz, A. M., Román-Berdiel, T., Oliva-Urcia, B., Soto, R., &

Aldega, L. (2018). Kinematics and strain distribution in an orogen-scale shear zone: Insights from structural analyses and magnetic fabrics in the Gavarnie thrust, Pyrenees. Journal of Structural Geology, 117(September), 105–123. https://doi.org/10.1016/j.jsg.2018.09.008Mulugeta, G., & Koyi, H. (1992). Episodic accretion and strain partitioning in a model sand wedge. Tectonophysics, 202, 319–333. https://doi.org/10.1016/0040-1951(92)90117-OMulugeta, Genene. (1988). Modelling the geometry of Coulomb thrust wedges. Journal of Structural Geology, 10(8), 847–859. https://doi.org/10.1016/0191-8141(88)90099-5Nilforoushan, F., Koyi, H. A., Swantesson, J. O. H., & Talbot, C. J. (2008). Effect of basal friction on surface and volumetric strain in models of convergent settings measured by laser scanner. Journal of Structural Geology, 30(3), 366–379. https://doi.org/10.1016/J.JSG.2007.09.013Parés, J. M., & van der Pluijm, B. A. (2004). Correlating magnetic fabrics with finite strain: Comparing results from mudrocks in the Variscan and Appalachian Orogens. Geologica Acta, 2(3), 213–220. https://doi.org/10.1344/105.000001428Parés, Josep M., & Van Der Pluijm, B. A. (2002). Evaluating magnetic lineations (AMS) in deformed rocks. Tectonophysics, 350(4), 283–298. https://doi.org/10.1016/S0040-1951(02)00119-1Parés, Josep M., Van der Pluijm, B. A., & Dinarès-Turell, J. (1999). Evolution of magnetic fabrics during incipient deformation of mudrocks (Pyrenees, northern Spain). Tectonophysics, 307(1–2), 1–14. https://doi.org/10.1016/S0040-1951(99)00115-8Ramsay, J. G., & Huber, M. I. (1983). The techniques of modern structural geology. Volume 1: strain analysis. The Techniques of Modern Structural Geology. Volume 1: Strain Analysis. https://doi.org/10.1016/0040-1951(86)90091-0Rochette, P., Jackson, M., & Aubourg, C. (1992). Rock Magnetism and the Interpretation of AMS, (92), 209–226.Saint-Bezar, B., Hebert, R. L., Aubourg, C., Robion, P., Swennen, R., & Frizon De Lamotte, D. (2002). Magnetic fabric and petrographic investigation of hematite-bearing sandstones within ramp-related folds: Examples from the South Atlas Front (Morocco). Journal of Structural Geology, 24(9), 1507–1520. https://doi.org/10.1016/S0191-8141(01)00140-7Sans, M., Vergés, J., Gomis, E., Parés, J. M., Schiattarella, M., Travé, A., et al. (2003). Layer parallel shortening in salt-detached folds: Constraint on cross-section restoration. Tectonophysics, 372(1–2), 85–104. https://doi.org/10.1016/S0040-1951(03)00233-6Schellart, W. P., & Strak, V. (2016). A review of analogue modelling of geodynamic processes: Approaches, scaling, materials and quantification, with an application to subduction experiments. Journal of Geodynamics, 100, 7–32. https://doi.org/10.1016/j.jog.2016.03.009Schöfisch, T., Koyi, H., & Almqvist, B. (2021). Influence of décollement friction on anisotropy of magnetic susceptibility in a fold-and-thrust belt model. Journal of Structural Geology, 144(September 2020). https://doi.org/10.1016/j.jsg.2020.104274Schöfisch, Thorben (2021), "popupStructure_3AnalogModels_MagneticFabricDistr", Mendeley Data, v1 http://dx.doi.org/10.17632/zs7n4t57k4.1Storti, F., Salvini, F., & McClay, K. (2000). Synchronous and velocity-partitioned thrusting and thrust polarity reversal in experimentally produced, doubly-vergent thrust wedges: Implications for natural orogens. Tectonics, 19(2), 378–396.

https://doi.org/10.1029/1998TC001079Suppe, J. (1983). Geometry and kinematics of fault-bend folding. American Journal of Science, 283(7), 684–721. https://doi.org/10.2475/ajs.283.7.684Teh-Quei Lee, Kissel, C., Laj, C., Chorng-Shern Horng, & Yi-Teh Lue. (1990). Magnetic fabric analysis of the Plio-Pleistocene sedimentary formations of the Coastal Range of Taiwan. Earth and Planetary Science Letters, 98(1), 23–32. https://doi.org/10.1016/0012-821X(90)90085-C

Tectonics

Supporting Information for

Magnetic fabric analysis along different parts of a thrust imbricate; a modelling approach

Thorben Schöfisch *[a], Hemin Koyi [a], Bjarne Almqvist [a]

[a] Department of Earth Sciences, Uppsala University, Villavägen 16, 75236 Uppsala, Sweden

* corresponding author: thorben.schofisch@geo.uu.se

Contents of this file

Figures S1 to S8

Introduction

This supplementary material contains additional figures for the publication. The figures show the distribution of the degree of anisotropy (S1), the shape of anisotropy (S2), the declination (S3-5) and inclination of the principal axes (S6-8) for each model in detail. The data are plotted on a representative section for each model. Note, that neither the size of the symbols nor the length and height of the model are scaled.

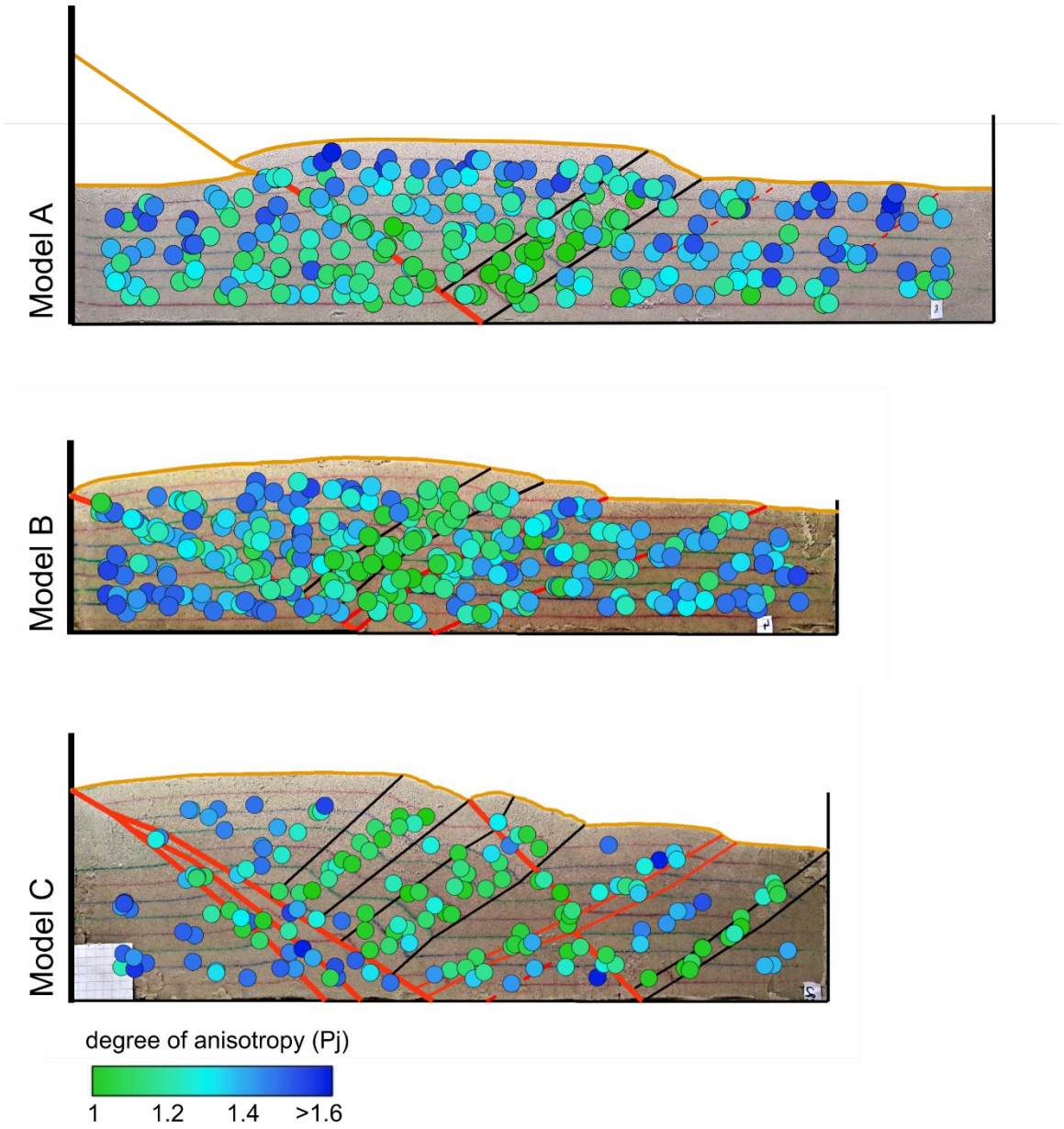

Figure S1. Distribution of the degree of anisotropy (*Pj*) plotted on a representative profile for each model.

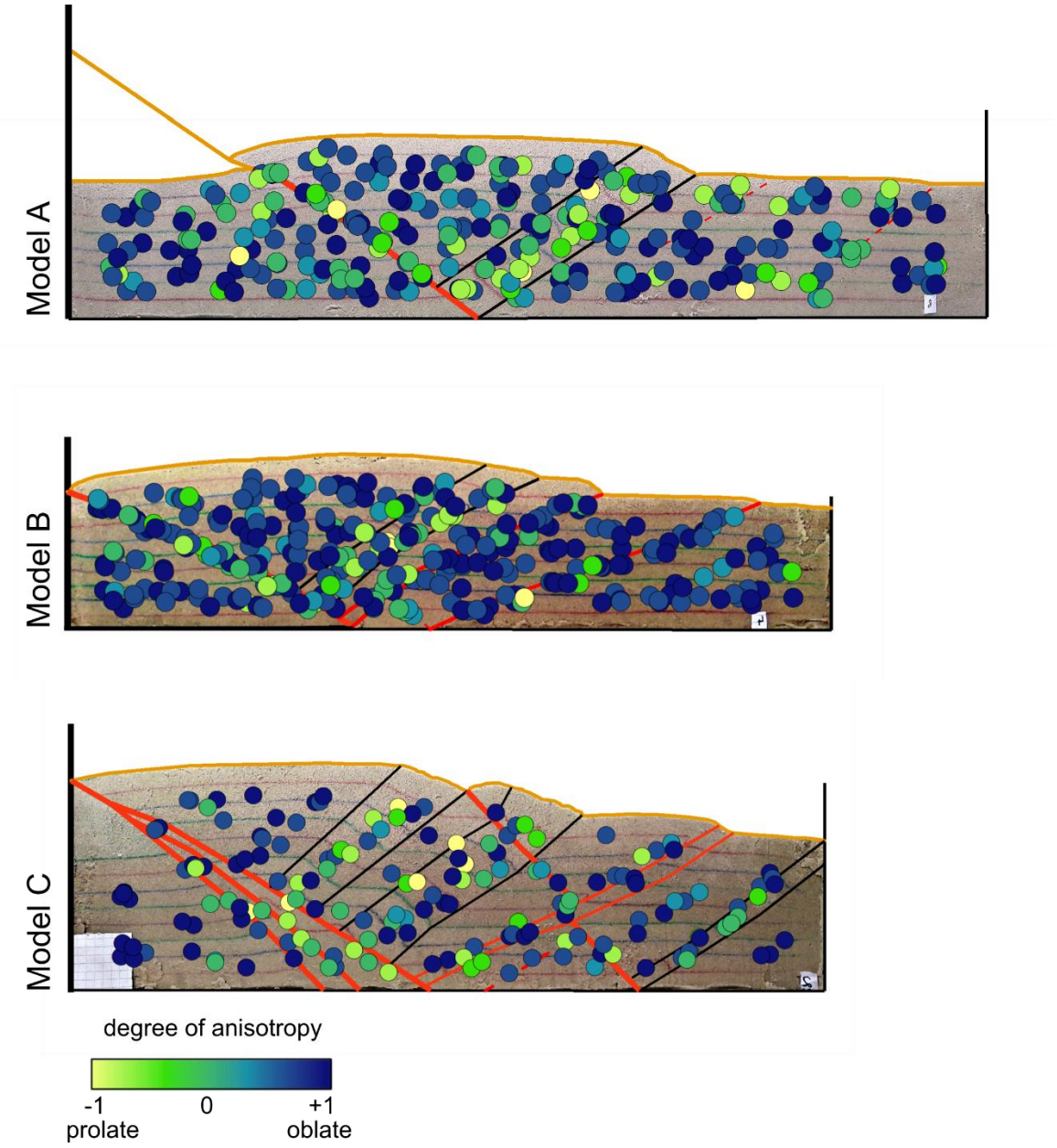

Figure S2. Distribution of the shape of anisotropy (*T*) plotted on a representative profile for each model.

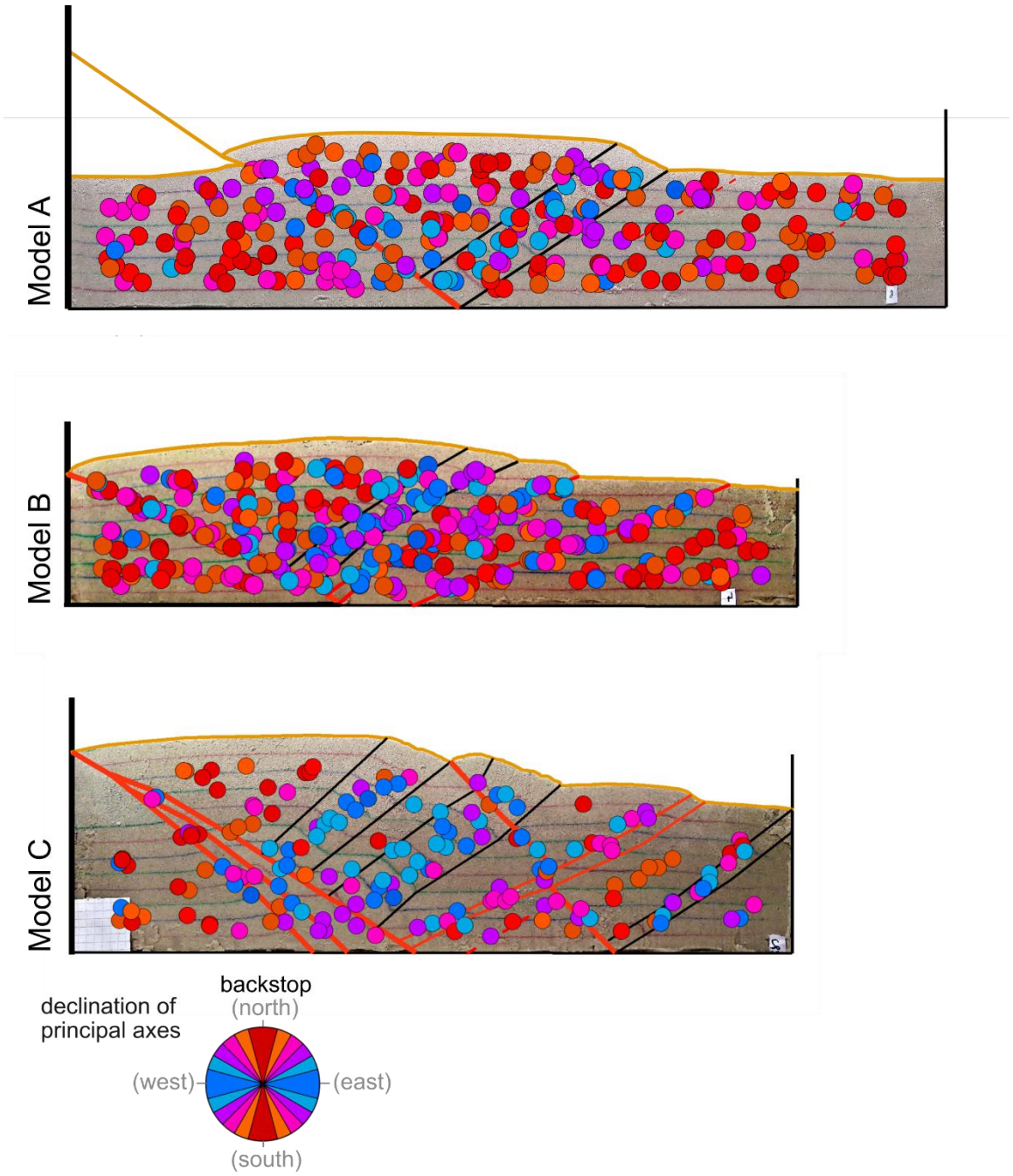

Figure S3. Distribution of k_{max} declination plotted on a representative profile for each model.

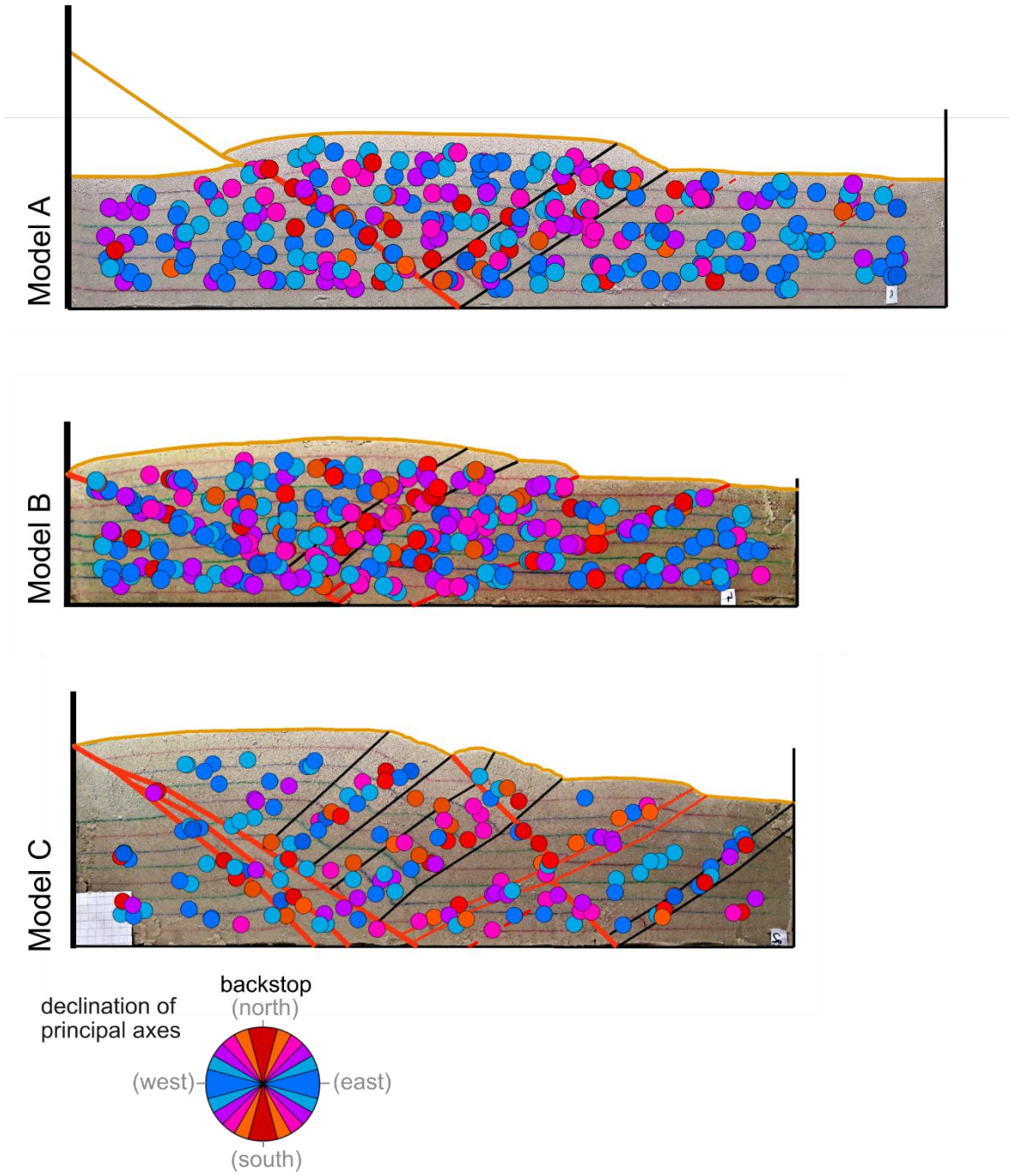

Figure S4. Distribution of k_{int} declination plotted on a representative profile for each model.

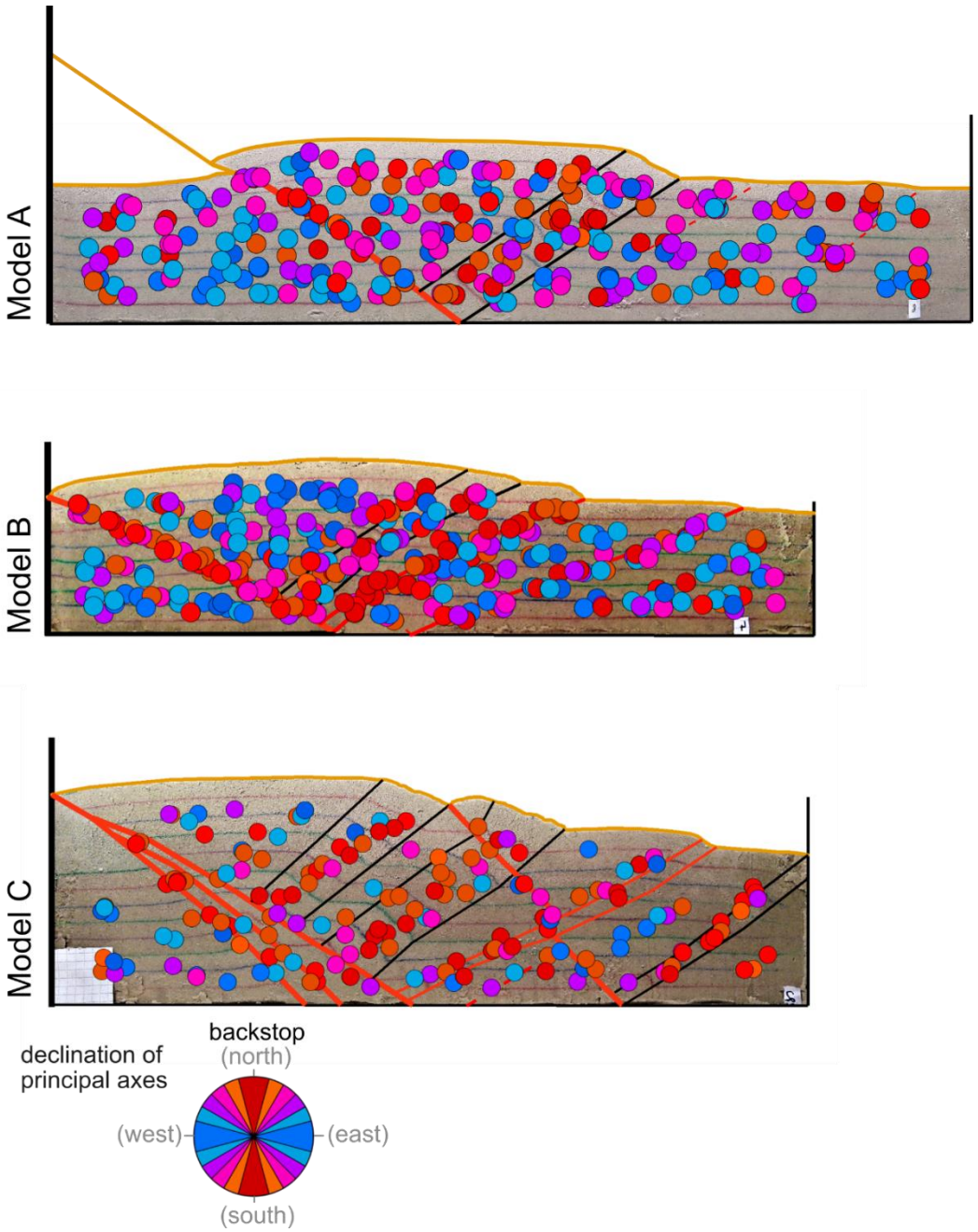

Figure S5. Distribution of k_{min} declination plotted on a representative profile for each model.

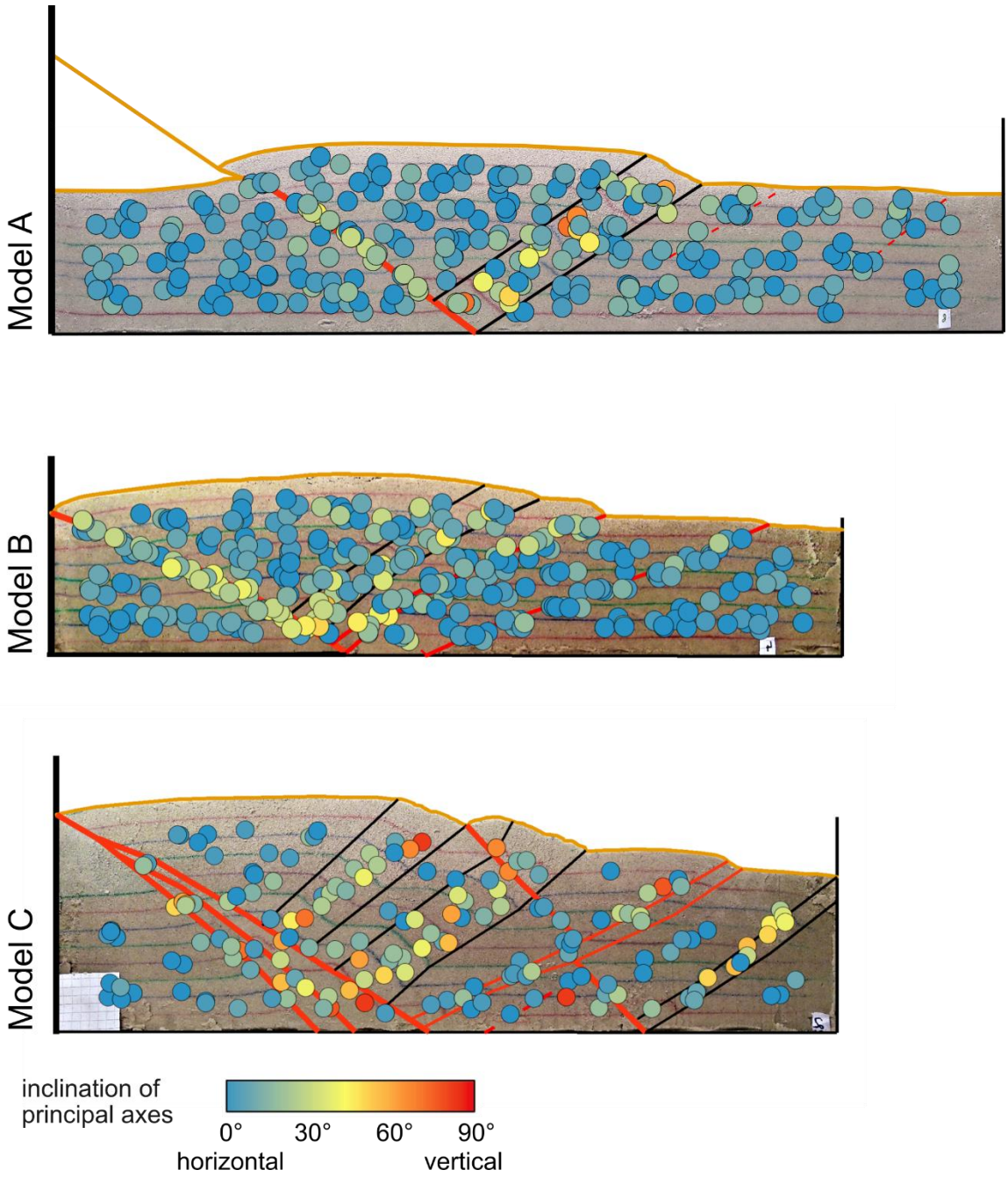

Figure S6. Distribution of k_{max} inclination plotted on a representative profile for each model.

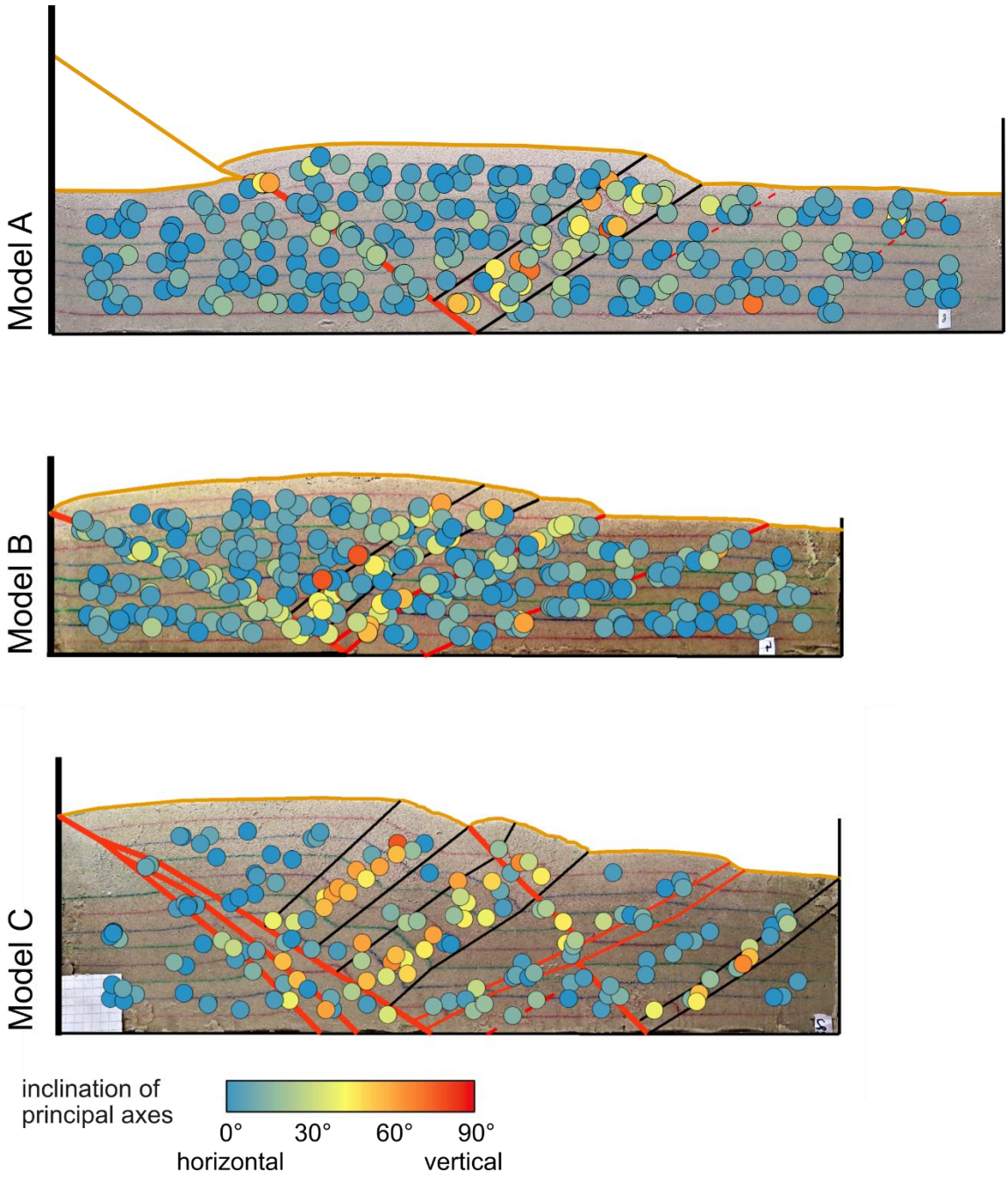

Figure S7. Distribution of k_{int} inclination plotted on a representative profile for each model.

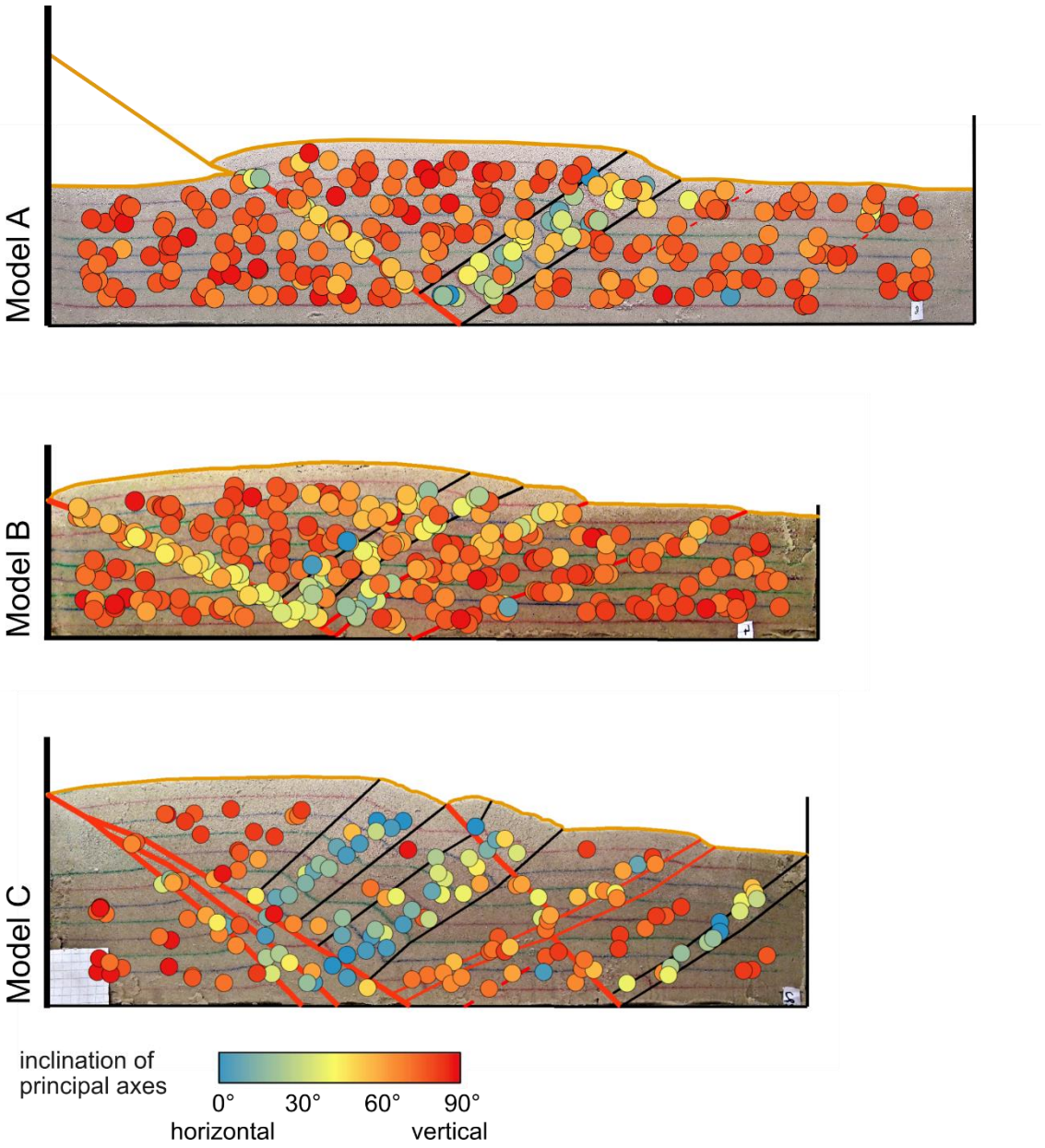

Figure S8. Distribution of k_{min} inclination plotted on a representative profile for each model.